Lunar Outgassing, Transient Phenomena & the Return to the Moon II: Predictions and Tests for Outgassing/Regolith Interactions

Arlin P.S. Crotts and Cameron Hummels

Department of Astronomy, Columbia University, Columbia Astrophysics Laboratory, 550 West 120th Street, New York, NY 10027

ABSTRACT

We follow Paper I with predictions of how gas leaking through the lunar surface could influence the regolith, as might be observed via optical Transient Lunar Phenomena (TLPs) and related effects. We touch on several processes, but concentrate on low and high flow rate extremes, perhaps the most likely. We model explosive outgassing for the smallest gas overpressure at the regolith base that releases the regolith plug above it. This disturbance's timescale and affected area are consistent with observed TLPs; we also discuss other effects.

For slow flow, escape through the regolith is prolonged by low diffusivity. Water, found recently in deep magma samples, is unique among candidate volatiles, capable of freezing between the regolith base and surface, especially near the lunar poles. For major outgassing sites, we consider the possible accumulation of water ice. Over geological time ice accumulation can evolve downward through the regolith. Depending on gases additional to water, regolith diffusivity might be suppressed chemically, blocking seepage and forcing the ice zone to expand to larger areas, up to km^2 scales, again, particularly at high latitudes.

We propose an empirical path forward, wherein current and forthcoming technologies provide controlled, sensitive probes of outgassing. The optical transient/outgassing connection, addressed via Earth-based remote sensing, suggests imaging and/or spectroscopy, but aspects of lunar outgassing might be more covert, as indicated above. TLPs betray some outgassing, but does outgassing necessarily produces TLPs? We also suggest more intrusive techniques from radar to in-situ probes. Understanding lunar volatiles seems promising in terms of resource exploitation for human exploration of the Moon and beyond, and offers interesting scientific goals in its own right. Many of these approaches should be practiced in a pristine lunar atmosphere, before significant confusing signals likely to be produced upon humans returning to the Moon.

1. Introduction

Transient lunar phenomena (TLPs or LTPs) are defined for the purposes of this investigation as localized (smaller than a few hundred km across), transient (up to a few hours duration, and probably longer than typical impact events - less than 1s to a few seconds), and presumably confined to processes near the lunar surface. How such events are manifest is summarized by Cameron (1972). In Paper I (Crotts 2008; see also Crotts 2009) we study the systematic behavior (especially the spatial distribution) of TLP observations - particularly their significant correlations with tracers of lunar surface outgassing, and we are thereby motivated to understand if this correlation is directly causal.

Numerous works have offered hypotheses for the physical cause of TLPs (Mills 1970, Garlick et al. 1972a, b, Geake & Mills 1977, Cameron 1977, Middlehurst 1977, Hughes 1980, Robinson 1986, Zito 1989, Carbognani 2004, Davis 2009), but we present a methodical examination of the influence of outgassing, exploring quantitatively how outgassing might produce TLPs. Furthermore, it seems likely that outgassing activity is concentrated in several areas, which leads one to ask how outgassing might interact with and alter the regolith presumably overlying the source of gas. Reviews of similar processes exist but few integrate Apollo-era data e.g., Stern (1999), Mukherjee (1975), Friesen (1975).

As the final version of this paper approached completion, several papers were published regarding the confirmed discovery of hydration of the lunar regolith. Fortunately, we deal here with the special effects of water on lunar regolith and find that many of our predictions are borne out in the recently announced data. We will deal with this explicitly in §5.

Several experiments from Apollo indicate that gas is produced in the vicinity of the Moon, even though these experiments disagree on the total rate: 1) LACE (Lunar Atmosphere Composition Experiment on *Apollo 17*), $\sim$0.1 g s^{-1} over the entire lunar surface (Hodges et al. 1973, 1974); 2) SIDE (Suprathermal Ion Detector Experiment on *Apollo 12, 14, 15*), $\sim$7 g s^{-1} (Vondrak et al. 1974); 3) CCGE (Cold Cathode Gauge Experiment on *Apollo 12, 14, 15*), $\lesssim$60 g s^{-1} (Hodges et al. 1972). These measurements not only vary by more than two orders of magnitude but also in assayed species and detection methods. LACE results here applies only to neutral ^{40}Ar, ^{36}Ar and ^{20}Ne. By mass ^{40}Ar predominates. SIDE results all relate to ions, and perhaps include a large contribution from molecular species (Vondrak et al. 1974). CCGE measures only neutral species, not easily distinguishing between them.

The LACE data indicate ^{40}Ar episodic outgassing on timescales of a few months or less (Hodges & Hoffman 1975), but resolving this into faster timescales is more ambiguous. In this discussion we adopt the intermediate rate (SIDE), about 200 tonne y^{-1} for the total production of gas, of all species, ionized or neutral. The LACE is the only instrument to

provide compositional ratios, which also include additional, rarer components in detail. We will use these ratios and in some cases normalize them against the SIDE total.

Much of the following discussion is only marginally sensitive to the actual composition of the gas. For many components of molecular gas at the lunar surface, however, there is a significant possible contribution from cometary or meteoritic impacts, and a lesser amount from solar wind/regolith interactions. The influx of molecular gas from comets and meteorites are variously estimated, usually in the range of tonnes or tens of tonnes per year over the lunar surface (see Anders et al. 1973, Morgan & Shemansky 1991). Cometary contributions may be sporadically greater (Thomas 1974). Except for H_2, solar wind interactions (Mukhergee 1975) provide only a small fraction of the molecular concentration seen at the surface (which are only marginally detected: Hoffman & Hodges 1975). There is still uncertainty as to what fraction of this gas is endogenous. Current data do not succeed in resolving these questions, but we will return to consider them later in the context of gas seepage/regolith interactions.

In this paper we consider various effects of outgassing through the regolith, and find the most interesting simple effect occurs when the flow is high enough to cause disruption of the regolith by an explosion to relieve pressure (§2), which we compare to fluidization. Another interesting effect occurs when the gas undergoes a phase change while passing through the regolith (§3), which seems to apply only to water vapor. This leads primarily to the prediction of the likely production of subsurface ice, particularly in the vicinity of the lunar poles. These effects suggest a variety of observational/experimental approaches, which we summarize in §4. In §5 we discuss the general implications of these findings, with specific suggestions as to how these might guide further exploration, particularly in respect to contamination by anthropogenic volatiles. We also discuss the relevance of the predictions in §4 to very recent discoveries regarding lunar regolith hydration.

First, let us make a few basic points about outgassing and the regolith. One can easily picture several modes in which outgassing volatiles might interact with regolith on the way to the surface. These modes will come into play with increasing gas flow rate and/or decreasing regolith depth, and we simply list them with mneumonic labels along with descriptions:

1) choke: complete blockage below the regolith, meaning that any chemistry or phase changes occur within the bedrock/megaregolith;

2) seep: gas is introduced slowly into the regolith, essentially molecule by molecule;

3) bubble: gas is introduced in macroscopic packets which stir or otherwise rearrange the regolith (such as "fluidization" e.g., Mills 1969);

4) gulp: gas is introduced in packets whose adiabatic expansion deposits kinetic energy into regolith and cools the gas, which therefore might even undergo a phase change;

5) explode: gas is deposited in packets at base of the regolith leading to an explosion; and

6) jet: gas simply flows into the vacuum at nearly sound speed with little entrained material.

While the intermediate processes might prove interesting, the extreme cases are probably more likely to be in effect and will receive more of our attention. In fact choking behavior might lead to explosions or geysers, when the pressure blockage is released. Since these latter two processes involve primarily simple hydrodynamics (and eventually, newtonian ballistics), we will consider them first, and how they might relate to TLPs.

2. Explosive Outgassing

If outgassing occurs at a rate faster than simple percolation can sustain, and where regolith obstructs its path to the surface, the accumulation of the gas will disrupt and cause bulk motion of the intervening regolith. The outgassing can lift the regolith into a cloud in the temporary atmosphere caused by the event. The presence of such a cloud has the potential to increase the local albedo from the perspective of an outside observer due to increased reflectivity and possible Mie scattering of underlying regolith. Additionally, volatiles buried in the regolith layer could become entrained in this gas further changing the reflective properties of such a cloud. Garlick et al. (1972b) describe fluidization of lunar regolith, in which dust is displaced only temporarily and/or over small distances compared to ballistic trajectories, but we will assume that we are dealing with more rapid changes.

2.1. Model Explosion

Let us construct a simple model of explosive outgassing through the lunar surface. For such an event to occur, we assume a pocket of pressurized gas builds at the base of the regolith, where it is delivered by transport through the crust/megaregolith presumably via channels or cracks, or at least faster diffusion from below. Given a sufficient flow rate (which we consider below), gas will accumulate at this depth until its internal pressure is sufficient to displace the overlying regolith mass, or some event releases downward pressure e.g., impact, moonquake, incipient fluidization, puncturing a seal, etc. We can estimate the minimal amount of gas alone required to cause explosive outgassing by assuming that the internal energy of the buried gas is equal to the total energy necessary to raise the overlying cone of regolith to the surface. This “minimal TLP” is the smallest outgassing event likely to produce potentially observable disruption at a new site, although re-eruption through thinned regolith will require less gas.

We consider the outgassing event occurring in two parts illustrated in Figure 1. Initially, the gas bubble explodes upward propelling regolith with it until it reaches the level of the surface; we assume that the plug consists of a cone of regolith within 45° of the axis passing from the gas reservoir to the surface, normal to the surface. Through this process the gas and regolith become mixed, and we assume they now populate a uniform hemispherical distribution of radius $r \approx 14$ m on the surface. At this point, the gas expands into the vacuum and drags the entrained regolith outward until the dust cloud reaches a sufficiently small density to allow the gas to escape freely into the vacuum and the regolith to fall eventually to the surface. We consider this to be the "minimal TLP" for explosive outgassing, as there is no additional reservoir that is liberated by the event beyond the minimum to puncture the regolith. One could also imagine triggering the event by other means, many of which might release larger amounts of gas other than that poised at hydrodynamical instability.

For the initial conditions of the first phase of our model, we assume the gas builds up at the base of the regolith layer at a depth of 15 m (for more discussion of this depth, see §3). We set the bulk density of the regolith at 1.9 g cm^{-3} (McKay et al. 1991), thereby setting the pressure at this depth at 0.45 atm. Because of the violent nature of an explosive outgassing, we assume that the cone of dust displaced will be 45° from vertical (comparable to the angle of repose for a disturbed slope of this depth: Carrier, Olhoeft & Mendell 1991). The mass of overlying regolith defined by this cone is $m = 7 \times 10^6$ kg.

In order to determine the mass of gas required to displace this regolith cone, we equate the internal energy of this gas bubble with the potential energy ($U = mgh$, where $g = 1.62$ m s^{-2}) required to lift the cone of regolith a height $h = 15$ m to the surface, requiring 47,000 moles of gas. Much of the gas found in outgassing events consists of ^{4}He, ^{36}Ar and ^{40}Ar (see §1), so we assume a mean molar mass for the model gas of $\mu \approx 20$ g mol^{-1}, hence 940 kg of gas is necessary to create an explosive outgassing event. The temperature at this depth is ~ 0°C (see §3), consequently implying an overall volume of gas of 2400 m^3 or a sphere 8.3 m in radius. What flow rate is needed to support this?

Using Fick's diffusion law, $j = -K\, dn/dz$, where the gas number density $n = 1.1 \times 10^{19}$ cm^{-3} is taken from above, and drops to zero through 15 m of regolith in z. The diffusivity K is 7.7 and 2.3 cm^2 s^{-1} for He and Ar, respectively, in the Knudsen flow regime for basaltic lunar soil simulant (Martin et al. 1973[1]), so we adopt $K = 5$ cm^2 s^{-1} for our assumed He/Ar mixture. (For any other gas mixture of this molecular weight, K would likely be smaller;

[1]For the relatively nonreactive gases He and Ar, the diffusivity is proportional to $(T/\mu)^{1/2}$, where T is the absolute temperature. The sticking time of the gas molecules, or heat of absorption, becomes significant if the gas is more reactive or the temperature is reduced. Unfortunately we find no such numbers for real regolith, although we discuss realistic diffusivities for other gases below.

below we also show that K tends to be lower for real regolith.) Over the area of the gas reservoir, this implies a mass leakage rate of 2.8 g s^{-1}, or ∼40% of the total SIDE rate. With the particular approximations made about the regolith diffusivity, this is probably near the upper limit on the leakage rate. At the surface of the regolith, this flow is spread to a particle flux of only $\sim 10^{16}$ cm^{-2}, which presumably causes no directly observable optical effects. The characteristic time to drain (or presumably fill) the reservoir is 4 d.

The second phase of the simulation models the evolution of dust shells and expanding gas with a spherically symmetric 1D simulation centered on the explosion point. The steps of the model include: 1) The regolith is divided into over 600 bins of different mean particle size. These bins are logarithmically spaced over the range $d = 8$ mm to $d = 0.02\mu$m according to the regolith particle size distribution from sample 72141,1 (from McKay et al. 1974). The published distribution for sample 72141,1 only goes to 2μm, but other sources (Basu & Molinaroli 2001) indicate a component extending below 2μm, so we extend our size distribution linearly from 2μm to 0μm. Furthermore, we assume the regolith particles are spherical in shape and do not change in shape or size during the explosion; 2) To represent the volume of regolith uniformly entrained in the gas, we create a series of 1000 concentric hemispherical shells for each of the different particle size bins (i.e., roughly 600,000 shells). Each of these shells is now independent of each other and totally dependent on the gas-pressure and gravity for motion; 3) We further assume that each regolith shell remains hemispherical throughout the simulation. Explicitly, we trace the dynamics of each shell with a point particle, located initially 45 degrees up the side of the shell; 4) We calculate the outward pressure of the gas exerted on the dust shells. The force from this pressure is distributed among different shells of regolith particle size weighted by the total surface area of the grains in each shell. We calculate each shell's outward acceleration and consequently integrate their equations of motion using a timestep $dt = 0.001$ s; 5) We calculate the diffusivity of each radial shell (in terms of the ability of the gas to move through it) by dividing the total surface area of all dust grains in a shell by the surface area of the shell itself (assuming grains surfaces to be spherical); 6) Starting with the largest radius shell, we sum the opacities of each shell until we reach a gas diffusive opacity of unity. Gas interior to this radius cannot "see" out of the external regolith shells and therefore remains trapped. Gas outside of this unit opacity shell is assumed to escape and is dropped from the force expansion calculation. Dust shells outside the unit opacity radius are now assumed to be ballistic; 7) We monitor the trajectory of each dust shell (represented by its initially 45° particle) until it drops to an elevation angle of 30° (when most of the gas is expanding above the particle), at which time this particle shell is no longer supported by the gas, and is dropped from the gas-opacity calculation; 8) An optical opacity calculation is made to determine the ability of an observer to see the lunar surface when looking down on the cloud. We calculate the downward optical opacity (such as from Earth) by dividing the

total surface area of the dust grains in a shell by the surface area of the shell as seen from above (πr^2). Starting with the outmost dust shell, we sum downward-view optical opacities until we reach optical depth $\tau = 1$ and $\tau = 0.1$ to keep track the evolution of this cloud's appearance as seen from a distance; 9) We return to step #4 above and iterate another timestep dt, integrating again the equations of motion. We continue this algorithm until all gas is lost and all regolith has fallen to the ground.

Finally, when all dust has fallen out, we calculate where the regolith ejecta have been deposited. Because we're representing each shell as a single point for the purposes of the equations of motion calculations, we want to do more than simply plot the location of each shell-particle on the ground to determine the deposition profile of ejected regolith. Thus we create a template function for the deposition of a ballistic explosion of a single spherical shell of material. By applying this template to each shell-particle's final resting location, we better approximate the total deposition of material from that shell. We then sum all of the material from the $\approx 600,000$ shells to determine the overall dust ejecta deposition profile.

There are obvious caveats to this calculation. Undoubtably the release mechanism is more complex than that adopted here, but this release mode is sufficiently simple to be modeled. Secondly, the diffusion constant, and therefore the minimal flow rate, might be overestimated due to the significant (but still largely unknown) decrease in regolith porosity with increasing depth on the scale of meters (Carrier et al. 1991), plus the liklihood that simulants used have larger particles and greater porosity than typical regolith. Lastly, the regolith depth of 15 meters might be an overestimate for some of these regions, which are among the volcanically youngest and/or freshest impacts on the lunar surface. This exception does not apply to Plato and its active highland vicinity, however, and Aristarchus is thickly covered with apparent pyroclastic deposits which likely have different but unknown depths and diffusion characteristics.

2.2. Results from Explosive Outgassing Model

We find results for this "minimal TLP" numerical model of explosive outgassing through the lunar regolith interesting in terms of the reported properties of TLPs. Figure 2 shows the evolution of the model explosion with time, as might be seen from an observer above, in terms of the optical depth $\tau = 1$ and $\tau = 0.1$ profiles of the model event, where $\tau = 1$ is a rough measure of order unity changes in the appearance of the surface features, whereas $\tau = 0.1$ is close to the threshold of the human eye for changes in contrast, which is how many TLPs are detected (especially the many without noticable color change). In both cases the cloud at the particular τ threshold value expands rapidly to a nearly fixed physical extent,

and maintains this size until sufficient dust has fallen out so as to prevent any part of the cloud from obscuring the surface to this degree.

Easily-seen effects on features ($\tau = 1$) lasts for 50 s and extends over a radius of 2 km, corresponding to 2 arcsec in diameter, resolvable by a typical optical telescope but often only marginally so. In contrast, the marginally detectable $\tau = 0.1$ feature extends over 14 km diameter (7.5 arcsec), lasting for 90 s, but is easily resolved. This model "minimal TLP" is an interesting match to the reported behavior of non-instantaneous (not $\lesssim 1$ s) TLPs: about 7% of duration 90 s or less, and half lasting under about 1300 s. Certainly there should be selection biases suppressing reports of shorter events. Most TLP reports land in an envelope between about two minutes and one hour duration, and this model event lands at the lower edge of this envelope. Furthermore, most TLPs, particularly shorter ones, are marginally resolved spatially, as would be the easily-detectable component of the model event. This correspondence also seems interesting, given the simplicity of our model and the state of ignorance regarding relevant parameters.

How might this dust cloud actually affect the appearance of the lunar surface? First, the cloud should cast a shadow that will be even more observable than simple surface obscuration, blocking the solar flux from an area comparable to the $\tau = 1$ region and visible in many orientations. Experiments with agitation of lunar regolith (Garlick et al. 1972b) show that the reflectance of dust is nearly always increased under fluidization, typically by about 20% and often by about 50% depending on the particular orientation of the observer versus the light source and the cloud. Similar results should be expected here for our simulated regolith cloud. These increases in lunar surface brightness would be easily observable spread over the many square kilometers indicated by our model.

Furthermore, because the sub-micron particle sizes dominate the outer regions of the cloud, it seems reasonable to expect Mie-scattering effects in these regions with both blue and red clouds expected from different Sun-Earth-Moon orientations. Figure 3 shows the typical fall-out time of dust particles as a function of size. Particles larger than $\sim$30 μm all fall out within the first few seconds, whereas after a few tens of seconds, particles are differentiated for radii capable of contributing to wavelength-dedendent scattering. Later in the event we should expect significant color shifts (albeit not order-unity changes in flux ratios).

The larger dynamical effects in the explosion cloud change rapidly over the event. Half of the initially entrained gas is lost from the cloud in the first 3 s, and 99% is lost in the first 15 s. Throughout the observable event, the remaining gas stays in good thermal contact with the dust, which acts as an isothermal reservoir. Gas escaping the outer portions of the dust cloud does so at nearly the sound speed ($\sim$ 420 m s^{-1}), and the outer shells of dust

also contain particles accelerated to similar velocities. Gas escaping after about 3 s does so from the interior of the cloud in parcels of gas with velocities decreasing roughly inversely with time. One observable consequence of this is the expectation that much of the gas and significant dust will be launched to altitudes up to about 50 km, where it may be observed and might affect spacecraft in lunar orbit.

The longterm effects of the explosion are largely contained in the initial explosion crater (nominally 14 m in radius), although exactly how the ejecta ultimately settle in the crater is not handled by the model. At larger radii the model is likely to be more reliable; Figure 4 shows how much dust ejecta is deposited by the explosion as a function of radius. Beyond the initial crater, the surface density of deposited material varies roughly as $\mu \propto r^{-2.7}$, so it converges rapidly with distance. Inside a radius of $\sim$ 300 m, the covering factor of ejecta is greater than unity; beyond this one expects coverage to be patchy. This assumes that the crater explosion is symmetric and produces few "rays." The explosion can change the reflectivity by excavating fresh material. This would be evidenced by a $\sim$10% drop in reflectance at wavelength $\lambda \approx 950$ nm caused by surface Fe^{2+} states in pyroxene and similar minerals (Adams 1974, Charette et al. 1976). Likewise there is an increase in reflectivity in bluer optical bands (Buratti et al. 2000) over hundreds of nm. Even though these photometric effects are compositionally dependent, we are interested only in differential effects: gradients over small distances and rapid changes in time. The lifetime of even these effects at 300 m radius is short, however, due to impact "gardening" turnover. The half-life of the ejecta layer at 300 m radius is only of order 1000 y (from Gault et al. 1974), and shorter at large radius (unless multiple explosions accumulate multiple layers of ejecta). At 30 m radius the half-life is of order 10^6 y. From maturation studies of the 950 nm feature (Lucey et al. 2000, 1998), even at 30 m, overturn predominates over optical maturation rates (over hundreds of My).

The scale of outgassing in this model event, both in terms of gas release ($\gtrsim$ 1 tonne) and timescale ($\gtrsim$ 4 d), are consistent with the total gas output and temporal granularity of outgassing seen in ^{40}Ar, a dominant lunar atmospheric component. The fact that this model also recovers the scale of many features actually reported for TLPs lends credence to the idea that outgassing and TLPs might be related to each other causally in this way, as well as circumstantially via the Rn^{222} episodes and TLP geographical correlation (Paper I).

How often such an explosive puncturing of the regolith layer by outgassing should occur is unknown, due to the uncertainty in the magnitude and distribution of endogenous gas flow to the surface, and to some degree how the regolith reacts in detail to large gas flows propagating to the surface. Also, a new crater caused by explosive outgassing will change the regolith depth, its temperature structure, and eventually its diffusivity. We will not attempt here to follow the next steps in the evolution of an outgassing "fumerole" in this way, but

are inspired to understand how regolith, its temperature profile, and gas interact, as in the next section. Furthermore, such outgassing might happen on much larger scales, or might over time affect a larger area. Indeed, such a hypothesis is offered for the scoured region of depleted regolith forming the Ina D feature and may extend to other regions around Imbrium (Schultz et al. 2006).

Our results here and in Paper I bear directly on the argument of Vondrak (1977) that TLPs as outgassing events are inconsistent with SIDE episodic outgassing results. The detection limits from ALSEP sites *Apollo 12, 14* and *15* correspond to 16-71 tonne of gas per event at common TLP sites, particularly Aristarchus. (Vondrak states that given the uncertainties in gas transportation, these levels are uncertain at the level of an order of magnitude.) Our "minimal TLP event" described above is 20-80 times less massive than this, however, and still visible from Earth. It seems implausible that a spectrum of such events would never exceed the SIDE limit, but it is not so obvious such a large event would occur in the seven-year ALSEP operations interval. Also, this SIDE limit interpretation rests crucially on Alphonsus (and Ross D) as prime TLP sites, both features which are rejected by our robust geographical TLP sieve in Paper I.

2.3. Coronal Discharge Effects

Dust elutriation or particle segregation in a cloud agitated by a low-density gas, occurring in this model, could potentially generate large electrostatic voltages, perhaps relating to TLPs (Mills 1970). Luminous discharges are generated in terrestrial volcanic dust clouds (Anderson et al. 1965, Thomas et al. 2007). Above we see dust particles remain suspended in a gas of number density $n = 10^{10}$ to 10^{15} cm^{-3} on scales of several tenths of a km to several km, a plausible venue for large voltages. In the heterogeneous lunar regolith, several predominant minerals with differing particle size may segregate under gas flow suspension and acceleration. Assuming a typical particle size of $r = 10$ μm, and typical work function differences[2] of $\Delta W = 0.5$ eV, two particles exchange charge upon contact until the equivalent of ± 0.25V is maintained, amounting to $Q = CV = 4\pi\epsilon_0 rV = 2.8 \times 10^{-16}$ coul = 1700 e$^-$. When these particles separate to distance $d >> r$, their mutual capacitance becomes $C_2 = 4\pi\epsilon_0 r^2/d$. For $d = 100$ m, if particles retain Q, voltages increase by 10^7 times! Such

[2]Predicting actual values of ΔW for particles of even well-defined compositions is problematic due to surface effects such as solar-wind/micrometeoritic weathering and exposed surface Fe^{2+} states. The following analysis suffices for two particles of different conducting composition; a similar result arises via triboelectric interaction of two different dielectrics although the details are less understood. Disturbed dust is readily charged for long periods in the lunar surface environment (Stubbs, Vondrak & Farell 2005).

voltages cannot be maintained.

Paschen's coronal discharge curve reaches minimum potential at 137V for Ar, 156V for He, for column densities N of 3.2×10^{16} and 1.4×10^{17} cm^{-2}, respectively, and rises steeply for lesser column densities (and roughly proportional to N for larger N).[3] Similar optimal N are found for molecules, with minimum voltages a few times higher e.g., 420V at 1.8×10^{16} cm^{-2} for CO_2, 414V for H_2S, 410V for CH_4, and N for other molecules $\sim 2.1 \times 10^{16}$ cm^{-2}.

The visual appearance of atomic emission in high voltage discharge tubes is well know, with He glowing pink-orange (primarily at 4471.5Å and 5875.7Å: Reader & Corliss 1980, Pearse & Gaydon 1963), and Ar glowing violet (from lines 4159-4880Å). If this applies to TLPs, the incidence of intense red emission in some TLP reports (Cameron 1978) argues for another gas.[4] Ne is not an endogenous gas. Common candidate molecules appear white or violet-white (CO_2, SO_2) or red (water vapor - primarily Hα, which is produced in many hydrogen compounds; CH_4 - Balmer lines plus CH bands at 390 and 431 nm).

The initial gas density at the surface from a minimal TLP is $\sim 10^{18}$ cm^{-3}, so initially the optimal N for coronal discharge is on cm scales (versus the initial outburst over tens of meters). As the TLP expands to 1 km radius, n drops to $\sim 10^{13}$ cm^{-3}, so the optimal N holds over the scale of the entire cloud, likely the most favorable condition for coronal discharge. If gas kinetic energy converts to luminescence with, for instance, 2% efficiency, at this density this amounts to ~ 0.1 J m^{-3}, or 100 J m^{-2}, compared to the reflected solar flux of 100 W m^{-2}, capable of a visible color shift for several seconds. Perhaps a minimal TLP could sustain a visible coronal discharge over much of its ~ 1 min lifetime. These should also be observable on the nightside surface, too, since solar photoionization is seemingly unimportant in initiating the discharge, and there are additional factors to consider.[5]

---

[3]These results depend somewhat the electrode's structure and composition. In carefully controlled conditions, breakdown voltages in He as low as 20V are achieved (Compton, Lilly & Olmstead 1920).

[4]The events and their colors reported can be counted (although a variation in outcomes depending on how one categorizes mixed colors and other factors). Following Paper I, we divide the sample at year 1956 (the later composing 1/4 of the sample); after 1955/before 1956: red - 52/11, blue (or blue-green) - 0/7, violet - 3/5, yellow - 0/4, red-yellow - 0/3, brown - 0/2, orange - 1/2. Red is common (out of 894 reports total, not including those by Bartlett, which are largely blue), however, there is a statistically significant change after 1956, where about 1/5 of reports include red color, many associated with Aristarchus, presumably due to a shift in observer behavior rather than the physics of lunar events. At least 20 nightside TLPs are reported, usually a bright and/or variable spot, 8 at/near Aristarchus e.g., 1824 May 1, near Aristarchus "blinking light, 9th to 10th mag on dark side; 1881 February 3, near Aristarchus: "very bright, like an 8th mag star, pulsating;" 1789 May 29: "flickering spot on east edge of Grimaldi," etc. Earthshine lunar surface brightness is $\mu \approx 12$ to 13 (mag arcsec^{-2}) in V, compared to 3.4 at full Moon, so visible sources could be faint.

[5]The timescale predicted for this effect depends largely on assuming gas emission in a single burst.

3. Seepage of Gas Through the Regolith

Referring back to scenarios (2) and (3) in §1, the onset of fluidization (Mills 1969) marks the division between these two regimes of seepage and "bubbling" and has been studied (Siegal & Gold 1973, Schumm 1970). Although laboratory test are made with coarser sieve particulates and much thinner dust layers in 1 g gravity, we can scale the gas pressure needed for incipient fluidization by g^{-2} and thickness t^1 to find the threshold $P = 0.16$ atm (Siegal & Gold 1973). Correcting for less diffusive regolith, this pressure estimate is likely a lower limit. Below this pressure simple gas percolation likely predominates.

What processes occur during "simple" percolation? Were it not for phase changes of venting gas within the regolith, the composition of the gas might be a weak consideration in this paper (except for perhaps the molecular/atomic mass), and temperature would likely only affect seepage as $T^{1/2}$ in the diffusivity. Water plays a special role in this study (separate from concerns regarding resource exploitation or astrobiology), in that it is the only common substance encountering its triple point temperature in passing through the regolith, at least in many locations. In this case water might not contribute to overpressure underneath the regolith leading to explosive outgassing. This would also imply that even relatively small volatile flows containing water would tend to freeze in place and remain until after the flow stops. For water this occurs at 0.01°C, corresponding to 0.006 atm in pressure (the pressure dropping by a factor of 10 every ∼25°.)

Effectively, water is the only relevant substance to behave in this fashion. The next most common substances may be large hydrocarbons such as nonane or benzene, obviously not likely abundant endogenous effluents from the interior. Also H_2SO_4 reaches its triple point, but changes radically with even modest concentrations of water. A similar statement can be made about HNO_3, not a likely outgassing constituent. These will not behave as their pure state, either; this leaves only H_2O. Water (and sulfur) has been found in significant concentration in volcanic glasses from the deep lunar interior (Saal et al. 2008, Friedman et al. 2009), and has been liberated in large quantities in past volcanic eruptions. The measured quantities of tens of ppm imply juvenile concentrations of hundreds of ppm.

From the heat flow measurements at the *Apollo 15* and *17* lunar surface experiment (ALSEP) sites (Langseth & Keihm 1977), we know that just below the surface, the stable regolith temperature is in the range of 247-253K (dependent on latitude, of course), with

---

Eruptions might occur along a non-point source, or from gas backed up along the length of a channel, producing a prolonged eruption. Additional complications might include interaction of agitated dust and/or gas with the channel. Such interactions can also generate much ionized gas under moderate voltages e.g., via a mechanism similar to that in a capillaritron (Perel et al. 1981, Bautsch et al. 1994).

gradients (below 1-2 m) of 1.2-1.8 deg m^{-1}, which extrapolates to 0°C at $13 - 16$ m depths subsurface. With the exception of the outermost few centimeters, the entire regolith is below the triple point temperature and is too deep to be affected significantly by variations in heating over monthly timescales. This is an interesting depth, since in many areas the regolith is not quite this deep, as small as under a few meters near Lichtenberg (Schultz & Spudis 1983) and at the Surveyor 1 site near Flamsteed (Shoemaker & Morris 1970) to depths at Apollo sites (summarized by McKay et al. 1991) near the 0°C depths calculated above, up to probably 20 m or more in the highlands, and 40 m deep north of the South Pole-Aitken Basin (Bart & Melosh 2005). Presumably, the fractured megaregolith supporting the regolith likely does not contain as many small particles useful for retaining water ice, as we detail below, but it may accumulate ice temporarily. Recent heat flow analyses (Saito et al. 2007) account for longer timescale fluctuations placing the 0°C depth twice as far subsurface, increasing the lifetime of retained volatiles against sublimation accordingly; for now we proceed with a more conventional, shorter-lived analysis.

The escape of water and other volatiles into the vacuum is regulated by the state of the regolith and is presumably largely diffusive. We assume the Knudsen flow regime (low-density, non-collisional gas). Of special importance is the measured abundance of small dust grains in the upper levels of the regolith, which perhaps pertains to depths ~ 15 m (where bulk density is probably higher: Carrier et al. 1991). Assuming that particle distributions are self-similar in size distribution (constant porosity), for random-walk diffusion out of a volume element dV, the diffusion time step presumably scales with the particle size a, so the diffusion time $t \propto a^{-1}$. For particles of the same density, therefore, one should compute the diffusion time by taking a a^{-1}-weighted average of particle sizes counted by mass, $\langle a \rangle$. This same moment of the distribution is relevant in §2.

Published size distributions measured to sufficiently small sizes include again McKay et al. (1974) with $\langle a \rangle = 24$ μm, and supplemented on smaller sizes with *Apollo 11* sample 10018 (Basu & Molinaroli 2001), which reduces the average to about 20 μm. This is an overestimate because a large fraction (34-63%) are agglutinates, which are groupings of much smaller particles. Many agglutinates have large effective areas e.g., $e = A/4\pi r^2$, with values of a few up to 8. (Here r is a mean radius from the center of mass to a surface element.) To a gas particle, the sub-particle size is more relevant than the agglutinate size, so the effective particle size of the entire sample might be much smaller, conceivably by a factor of a few.

We compare this to experimental simulations, a reasonably close analogy being the sublimation of a slab of ice buried up to 0.2 m below a medium of simulant JSC Mars-1 (Allen et al. 1998) operating at ~ 263°K and 7 mbar (Chevrier et al. 2007), close to lunar regolith conditions. This corresponds to the lifetime of 800 y for a 1 m thick ice layer covered

by 1 m of regolith. The porosity of JSC Mars-1 is 44-54%, depending on compactification whereas lunar soil has ∼49% at the surface, perhaps 40% at a depth of 60 cm, and slightly lower at large depths (Carrier et al. 1991). Lunar soil is somewhat less diffusive by solely this measure. The mean size $\langle a \rangle$ of JSC Mars-1 is 93 μm, $\gtrsim$10 times larger than that for *Apollo 17* and *11* regolith, accounting for agglutinates, so the sublimation timescale for regolith material is, very approximately, $\gtrsim$10 ky (perhaps up to ∼30 ky). Other simulants are more analogous to lunar regolith, so future experiments might be more closely relevant.

Converting a loss rate for 1 m below the surface to 15 m involves the depth ratio R. Farmer (1976) predicts an evaporation rate scaling as R^{-1} (as opposed to the no-overburden analysis: Ingersoll 1970). Experiments with varying depths of simulated regolith (Chevrier et al. 2007) show that the variation in lifetime indeed goes roughly as R^1, implying a 1 m ice slab lifetime at 15 m on the order of 10^5 to 3×10^5 y. The vapor pressure for water ice drops a factor of 10 in passing from 0°C to current temperatures of about −23°C just below the surface (also the naked-ice sublimation rate: Andreas 2007), which would indicate that ∼90% of water vapor tends to stick in overlying layers (without affecting the lifetime of the original layer, coincidentally). This begs the question of the preferred depth for an ice layer to form. The regolith porosity decreases significantly between zero and 1 m depth (Carrier et al. 1991) which argues weakly for preferred formation at greater depth. At 30 m depth or more, the force of overburden tends to close off porosity.

The current best limit on water abundance is from the sunrise terminator abundances from LACE, which produces a number ratio of $H_2O/^{40}Ar$ with a central value of 0.014 (with 2σ limits of 0-0.04). This potentially indicates an actual $H_2O/^{40}Ar$ outgassing rate ratio up to 5 times higher (Hoffman & Hodges 1975). Adopting the SIDE rate of 7 g s^{-1} in the ∼20-44 AMU mass range, and assuming most of this is ^{40}Ar (Vondrak, Freeman & Lindeman 1974: given the much lower solar wind contributions of other species in this range), this translates to 0.1 g s^{-1} of water (perhaps up to 0.5 g s^{-1} or 15 tonne y^{-1}), in which case most of the gas must be ionized. The disagreement between SIDE and LACE is a major source of uncertainty (perhaps due to the neutral/ionized component ambiguity).

We discuss below that at earlier times the subsurface temperature was likely lower, but let us consider now the situation in which a source arises into pre-established regolith in recent times. We assume a planar diffusion geometry, again. In this case, we take spatial gradients over 15 m and scale the JSC Mars-1 diffusivity of 1.7 cm^2 s^{-1} to 0.17 cm^2 s^{-1} for lunar regolith. Since the triple-point pressure corresponds to number density $n = 2.4 \times 10^{17}$ cm^{-3}, the areal particle flux density is $j = 2.7 \times 10^{13}$ s^{-1} cm^{-2}. For a large outgassing site, with the same water fraction of water indicated by LACE e.g., total outgassing of 7 g s^{-1} including 0.1 g s^{-1} of water, this rate can maintain a total area of 0.012 km^2 at the triple-point pressure i.e., a 125 m diameter patch. This is much larger than the 15 m regolith

depth, bearing out our assumed geometry. If this ice patch were 1 m thick, for example, the ice would need to be replenished every 4000 y.

Of course, this is a simple model and many complications could enter. We consider briefly the effects of latitude, change in lunar surface temperature over geological time, and the effects of aqueous chemistry on the regolith.

3.1. Latitude Effects

The temperature just below the surface is legislated by the time-averaged energy flux in sunlight, so it scales according to the Stefan-Boltzmann law from the temperature at the equator ($\phi = 0$) according to $T(\phi) = T(0)cos^{1/4}(\phi)$. This predicts a 6K temperature drop from the equator (at about 252K) to the latitude of the Aristarchus Plateau ($\phi \approx 26°$) or the most polar subsurface temperature measurement by *Apollo 15*, a drop to 224K at Plato ($\phi = 51°.6$), $\lesssim$200K for the coldest 10% of the lunar surface ($\phi > 65°$) and $\lesssim$150K for the coldest 1% ($\phi > 82°$).[6] These translate into a regolith depth at the water triple-point of $\sim$4, 18, 33 or 65 m deeper than at the equator, respectively, probably deeper in the latter cases than the actual regolith layer. Permanently shadowed cold traps, covering perhaps 0.1% of the surface, have temperatures $\lesssim$60K (e.g., Adorjan 1970, Hodges 1980). (Note that the lunar South Pole is a minor TLP site responsible for about 1% of robust report counts.) Since even at the equator the H_2O triple point temperature occurs $\sim$13 m below the surface, at increasing latitude this zone quickly moves into the megaregolith where the diffusivity is largely unknown but presumably higher (neglecting the decrease in porosity due to compression by overburden). To study this, we assume a low diffusivity regolith layer 15 m deep overlying a high diffusivity layer which may contain channels directing gas quickly upward (although perhaps not so easily horizontally).

The diffusivity of the regolith near 0°C is dominated by elastic reflection from mineral surfaces, without sticking, whereas at lower temperatures H_2O molecules stick during most collisions (Haynes, Tro & George 1992). This is especially the case if the surfaces are coated with at least a few molecular layers of H_2O molecules, of negligible mass. The sticking behavior of H_2O molecules on water ice has been studied over most of the temperature range relevant here (Washburn et al. 2003); but does depend somewhat on whether the ice is crystalline or amorphous (Speedy et al. 1996). In contrast the sticking behavior of H_2O molecules on lunar minerals is much less well known.

The lunar simulant diffusivity value above corresponds to a mean free path time of $\sim$1

[6]The most polar maria edge might border Frigoris at $\phi \approx 65°$, but there are flooded craters much higher.

μs for H_2O molecules near 0°C. In contrast the timescale for H_2O molecules sticking on ice is (from Schorghofer & Taylor [2007] and references therein): $\tau = \theta/(\alpha P_v/\sqrt{2\pi kT\mu})$, where θ is the areal density of H_2O molecules on ice $\theta = (\rho/\mu)^{2/3} \approx 10^{15}$ cm^{-2} for density ρ, and molecular mass μ. The sticking fraction α varies from about 70% to 100% for $T = 40$K to 120K. The equilibrium vapor pressure is given by $P_v = p_t\ exp[-Q(\frac{1}{T} - \frac{1}{T_t})/k]$ where p_t and T_t are the triple point pressure and temperature, respectively, and sublimation enthalpy $Q =$ 51.058 kJ/mole. This expression and laboratory measurements imply a sticking timescale $\tau \approx 1$ μs at $T = 260$K, 1 ms at 200K, 1 s at 165K, 1 hr at 134K, and 1 yr at 113K. The sticking timescale quickly and drastically overwhelms the kinetic timescale at lower temperatures.

This molecular behavior has a strong effect on the size of the ice patch maintained by the example source considered above. Simply scaling by the time between molecular collisions, corresponding to a 125 m diameter ice patch at $\phi = 0$, we find at the base of the regolith a 160 m patch at $\phi = 26°$ (Aristarchus Plateau), 580 m at $\phi = 51°.6$ (Plato), 2.3 km at $\phi = 65°$ (10% polar cap), and an essentially divergent value, 522 km at $\phi = 82°$ (1% polar cap). If in fact the regolith layer is much deeper than suspected, the added depth of low diffusivity dust significantly increases the patch area: 170 m at $\phi = 26°$, 830 m at $\phi = 51°.6$, and 4 km at $\phi = 65°$. Figure 5 presents graphically how the growth of the ice patch varies with latitude, plus also the effects of flow rate and the assumed regolith depth.

3.2. Longterm Evolution

Most portions of the lunar surface have been been largely geologically inactive during the past 3 Gy or more (with some of the notable exceptions listed above). During this time several important modifications of the scenario above are relevant.

The current heat flow from the lunar interior, $j_{int} \approx 0.03$ W m^{-2} (Langseth et al. 1972, 1973), is only a 2×10^{-5} part of the solar constant, so it affects the temperature near the lunar surface at the level of only ~ 1.3 millidegree. There were times in the past, however, when interior heating likely pushed the temperature near the surface over 0°C.

A zero-degree zone near the maria presumably could not form until ∼3 Gy ago, probably sufficient for the Moon globally (see Spohn et al. 2001). After this the 0°C depth receded into the regolith, while the regolith layer was also growing. Simultaneously, the average surface temperature was cooler by ~ 15 degree due to standard solar evolution (Gough 1981 – perhaps 17° lower in the highlands at 4 Gy ago). Since the the thickness of regolith after 3 Gy ago grows at only about 1 m per Gy (Quaide & Oberbeck 1975), within the maria the 0°C depth sinks into bedrock/fractured zone. Whatever interaction and modification might be involved between the regolith and volatiles will proceed inwards, leaving previous epochs'

effects between the surface vacuum and the 0°C layer now at $\sim$ 15 m.

3.3. Chemical Interactions with Regolith

Another issue to consider is possible regolithic chemical reactions with outgassing volatiles, especially over prolonged geological timescales. The key issue is the possible presence of water vapor, and perhaps SO_2. There is little experimental work on the aqueous chemistry of lunar regolith (which will vary due to spatial inhomogeneity). Dissolution of lunar fines by water vapor is greatly accelerated in the absence of other gases such as O_2 and N_2 (Gammage & Holmes 1975) and appears to proceed by etching the numerous damage tracks from solar-wind particles. This process acts in a way to spread material from existing grains without reducing their size (which would otherwise tend to increase porosity). Liquid water is more effective than vapor, not surprisingly, and ice tends to establish a pseudo-liquid layer on its surface. This is separate from any discussion of water retention on hydrated minerals surfaces robust to temperatures above 500°C (Cocks et al. 2002 & op cit.).

This is a complex chemical system that will probably not be understood without simulation experiments. The major constituents are presumably silicates, which will migrate in solution only over geologic time. (On Earth, consider relative timescales of order 30 My typical migration times for quartz, 700 ky for orthoclase feldspar, $KAlSi_3O_8$ and 80 ky for anorthite, $CaAl_2Si_2O_8$: Brantley 2004.) One might also expect the production of $Ca(OH)_2$, plus perhaps $Mg(OH)_2$ and $Fe(OH)_2$. It is not clear that $Fe(OH)_2$ would oxidize to more insoluble FeO(OH), but any free electrons would tend to encourage this. It seems that the result would be generally alkaline. Since feldspar appears to be a major component in some outgassing regions e.g., Aristarchus (McEwen et al. 1994), one should also anticipate the production of clays. This is not accounting for water reactions with other volatiles e.g., ammonia, which has been observed as a trace gas (Hoffman & Hodges 1975) perhaps in part endogenous to the Moon, and which near 0°C can dissolve in water at nearly unit mass ratio (also to make an alkaline solution). Carbon dioxide is a possible volatile constituent, and along with water can metamorphose olivine/pyroxene into $Mg_3Si_4O_{10}(OH)_2$ i.e. talc, albeit slowly under these conditions; in general the presence of CO_2 and thereby H_2CO_3 opens a wide range of possible reactions into carbonates. Likewise the presence of sulfur (or SO_2) opens many possibilities e.g., $CaSO_4{\cdot}2H_2O$ (gypsum), etc. Since we do not know the composition of outgassing volatiles in detail, we will probably need to inform simulation experiments with further remote sensing or in situ measurements.

The mechanical properties of this processed regolith are difficult to predict. Some possible products have very low hardness and not high ductility. Some of these products expand

but will likely fill the interstitial volume with material, which will raise its density and make it more homogeneous. Regolith is already ideal in having a nearly power-law particle distribution with many small particles. It seems likely that any such void-filling will sharply reduce diffusivity. The volatiles actually discovered in volcanic glasses from the deep interior (Saal et al. 2008, Friedman et al. 2009) include primarily H_2O and SO_2 but not CO_2 or CO. With the addition of water, regolithic mineral combinations tend to be cement-like, and experiments with anorthositic lunar chemical simulants have produced high quality cement without addition of other substances, except SiO_2 (Horiguchi et al. 1996, 1998). Whether this happens *in situ* depends upon whether over geological time $(CaO)_3SiO_2$ or other Ca can act as a binder without heating to sintering temperatures. The possible production of gypsum due to the high concentrations of sulfur would add to this cement-like quality. The extent to which ordinary mixes such as portland cement lose water into the vacuum depend on their content of expansive admixture (Kanamori 1995). Portland cement mixes show little evidence of loss of compressional strength in a vacuum (Cullingford & Keller 1992).

We need to think in terms of possibly cemented slabs in some vicinities, and need to consider the effects of cracks or impacts into this concrete medium. This is probably not a dominant process, since the overturn timescale to depths even as shallow as 1 m is more than 1 Gy (Gault et al. 1974, Quaide & Oberbeck 1975), whereas we discuss processes at $\sim$15 m or more. Craters 75 m in diameter will permanently excavate to a 15 m depth (e.g., Collins 2001, and ignoring the effects of fractures and breccia formation), and are formed at a rate of about 1 Gy^{-1} km^{-2} (extending Neukum et al. [2001] with a Shoemaker number/size power-law index 2.9). This will affect some of the areal scales discussed above, but not all. We speculate that vapor or solution flow might tend to deliver ice and/or solute to these areas and eventually act to isolate the system from the vacuum. Finally, we note above that over geological timescales this ice layer will tend to sink slowly into the regolith, at a rate of order 1 m Gy^{-1}, setting up a situation where any relatively impermeable concrete zone will tend to isolate volatiles from the vacuum. In this case volatile leakage will tend to be reduced to a peripheral region around the ice patch. Assuming that volatiles leak out through the entire 15 m thickness of regolith at the patch boundary, the 125 m diameter patch area for $\phi \approx 0$ from above corresponds to a peripheral zone expected from a 520 m diameter patch. Thus any such concrete overburden will encourage growth of small patches, and will do so even more for larger ones (assuming $\lesssim$15 m regolith depth).

How much water might reasonably be expected to outgas at these sites? The earliest analyses of Apollo samples argued for extreme scarcity of water and other volatiles (Anders 1970, Charles, Hewitt & Wones 1971, Epstein & Taylor 1972). On the Earth, water is the predominant juvenile outgassing component (Gerlach & Graeber 1985, Rubey 1964), whereas even the highest water concentrations discussed below (Saal et al. 2008) imply

values an order of magnitude smaller. On the Moon, water content is drastically smaller, with a current atmospheric water content much less than what would affect hydration in lunar minerals (Mukherkjee & Siscoe 1973), although some lunar minerals seem to involve water in their formation environments (Agrell et al. 1972, Williams & Gibson 1972, Gibson & Moore 1973, and perhaps Akhmanova et al. 1978). The origin of the water in volcanic glasses (Saal et al. 2008, Friedman et al. 2009) is still poorly understood but implies internal concentrations that at first look seems in contradiction with earlier limits e.g., Anders 1970. For much different lunar minerals, high concentration is implied for water (McCubbin et al. 2007) as well as other volatiles (Krähenbühl et al. 1973).

It is not a goal of this paper to explain detected water in lunar samples, but its origin at great depth is salient here. As a point of reference, Hodges and Hoffman (1975) show that the ^{40}Ar in the lunar atmosphere derives from deep in the interior, of order 100 km or more. They hypothesize that the gas could just as easily derive from the asthenosphere, 1000 km deep or more (see also Hodges 1977). The picritic glasses analyzed by Saal, Friedman, et al. derive from depths of ∼300-400 km or greater (Elkins-Tanton et al. 2003, Shearer, Layne & Papike 1994). O_2 fugacity measurements e.g., Sato 1979, are based on glasses from equal or lesser depths. Water originating from below the magma ocean might provide one explanation (Saal et al. 2008), as might inhomogeneity over the lunar surface. Differentiation might not have cleared volatiles from the deep interior despite its depletion partially into the mantle. One might also consider that geographical variation between terranes e.g., KREEP (K-Rare Earth Element-P) or not, might be important.

In the Moon's formation temperatures of proto-Earth and progenitor impactor material in simulations grow to thousands of Kelvins, sufficient to drive off the great majority of all volatiles, but these are not necessarily the only masses in the system. Either body might have been orbited by satellites containing appreciable volatiles, which would likely not be heated to a great degree and which would have had a significant probability of being incorporated into the final moon. Furthermore, there is recent discussion of significant water being delivered to Earth/Moon distances from the Sun in the minerals themselves (Lunine et al. 2007, Drake & Stimpfl 2007), and these remaining mineral-bound even at high temperatures up to 1000K (Stimpfl et al. 2007). The volume of surface water on Earth is at least 1.4×10^9 km^3, so even if the specific abundance of lunar water is depleted to 10^{-6} terrestrial, one should still expect over 10^{10} tonnes endogenous to the Moon, and it is unclear that later differentiation would eliminate this. This residual quantity of water would be more than sufficient to concern us with the regolith seepage processes outlined above.

For carbon compounds, models of the gas filling basaltic vesicles (Sato 1976; also O'Hara 2000, Wilson & Head 2003, Taylor 1975) predict CO, COS, and perhaps CO_2 as major components. Negligible CO_2 is found in fire-fountain glasses originating from the deep interior

(Saal et al. 2008); this should be considered in light of CO on the Moon (and CO_2 on Earth) forming the likely predominant gas driving the eruption (Rutherford & Papale 2009).

We suspect that water outgassing was likely higher in the past than it is now. Furthermore, no site of activity traced by ^{222}Rn or by robust TLP counts (Paper I) has been sampled. (The sample return closest to Aristarchus, *Apollo 12*, is 1100 km away.)[7] From our discussion above the behavior of outgassing sites near the poles versus near the equator might differ greatly, with volatile retention near the poles being long-term and perhaps making the processing of volatiles much more subterranean and covert. (Note that the lunar South Pole is a minor TLP site responsible for about 1% of robust report counts, as per Paper I.)

With these uncertainties we feel unable to predict exactly how or where particular evidence of lunar surface outgassing might be found, although the results from above offer specific and varied signals that might be targeted at the lunar surface. For this reason we turn attention to how such effects might be detected realistically from the Earth, lunar orbit, and near the Moon's surface, and we suggest strategies not only for how these might be tested but also how targeted observations might economically provide vital information about the nature of lunar outgassing. We consider the impact of recent hydration detections in §5.

We appreciate the controversial nature of suggesting small but significant patches of subsurface water ice, given the history of the topic. We take care to avoid "cargo cult science" - selection of data and interpretion to produce dramatic but subjectively biased conclusions that do not withstand further objective scrutiny (Feynman 1974). Despite the advances made primarily by Apollo-era research, we are still skirting the frontiers of ignorance. We are operating in many cases in a regime where interesting observations have been made but the parameters e.g., the endogenous lunar molecular production (water vapor or otherwise), required to evaluate alternative models and interpretations are sufficiently uncertain to frustrate immediate progress. Below we offer several straightforward and prompt tests of our conclusions and hypotheses which offer prospects of settling many of these issues.

---

[7]The only persistent TLP site of some statistical significance that corresponds to a sample return (170 g from *Luna 24*) is Mare Crisium, ambiguous in several ways: 1) the robust TLP report count for Crisium is only zero to 6, depending on the robustness filter employed (Paper I); 2) the nature of this robust count is problematic given the extended nature of Crisium as a feature, and 3) the 2-meter core sample returned from Crisium by *Luna 24* is one case where the presence of significant water may be indicated (Akhmanova et al. 1978).

4. Observational and Experimental Techniques

TLPs are rare and short-lived, which hampers their study. We advance supplanting the current anecdotal catalog with data with *a priori* explicit, calculable selection effects. This might seem daunting; Paper I used in essence all known reports from lunar visual observers since the telescope's invention! With modern imaging and computing, it is tractable.

Another problem clear above is the variety of ways in which outgassing can interact with the regolith. In cases of slow seepage, gases may long delay their escape from the regolith. If the gases are volcanic, they might interact along the way, and water vapor might trap it and other gases in the regolith. These factors bear on designing future investigations.

We can make significant headway exploiting more modern technology. Table 1 lists the many methods detailed in this section. There has been no areal-encompassing, digital image monitoring of the Near Side with appreciable time coverage using modern software techniques to isolate transients. Numerous particle detection methods are promising. The relevant experiments on Apollo were limited in duration, a week or less, or 5-8 years in the case of ALSEP. Furthermore *Clementine* and the relevant portion of *Lunar Prospector* were also relatively short. These limitations serve as background to the following discussions. In this section we provide a potential roadmap to detailed study of outgassing.

4.1. Optical/Infrared Remote Sensing

Optical imaging advances several goals. Transient monitoring recreates how TLPs were originally reported. Not yet knowing TLP emission spectra, our bandpass should span the visual, 400-700 nm. After an event, surface morphology/photometry changes might persist, betrayed by 0.95 and 1.9 μm surface Fe^{2+} bands and increased blue reflectivity (§2.2). Hydration is manifest in the infrared. Asteroidal regolith 3 μm hydration signals are common (Lebofsky et al. 1981, Rivkin et al. 1995, 2002, Volquardsen et al. 2004), and stronger than those at 700 nm (Vilas et al. 1999) seen in lunar polar regions. Absorption near 3 μm appears in lunar samples exposed to terrestrial atmosphere for a few years (Markov et al. 1980, Pieters et al. 2005) but not immediately (Akhmanova et al. 1972), disappearing within a few days in a dry environment. Further sample experiments are needed.

4.1.1. Earth-Based Imaging

Earth-based monitoring favors the Near Side, as do TLP-correlated effects: ^{222}Rn outgassing (all four events on nearside, plus most ^{210}Po residual) and mare edges. The best,

consistent resolution comes from the *Hubble Space Telescope* with $0.07-0.1$ arcsec FWHM ($\sim$150 m) but with large overhead times. Competing high-resolution imaging from "Lucky Exposures" (LE, also "Lucky Imaging") exploits occasionally superlative imaging within a series of rapid exposures (Fried 1978, Tubbs 2003). Amateur setups achieve excellent LE results, and the Cambridge group (Law, Mackay & Baldwin 2006) attains diffraction-limited imaging on a 2.5-meter telescope, $\sim$200-300 m FWHM. Only $<$1% of observing time survives image selection, but for the Moon this requires little time. LE resolution is limited to a seeing isoplanatic patch, $\sim$1000 arcsec^2, 3000 times smaller than the Moon. Likewise, *HST*'s Wide Field Camera 3, covering 3000 arcsec^2, cannot practically survey the Near Side.

High resolution imaging can monitor small areas over time or in one-shot applications compared with other sources i.e., lunar imaging missions. LE or *HST* match the resolution of global maps from *Lunar Reconnaissance Orbiter* Camera's (LROC) Wide-Angle Camera (Robinson et al. 2005), and *Clementine*/UVIS, over 0.3-1 μm. *Kaguya*'s Multiband Imager (Ohtake et al. 2007) has 40-m 2-pixel resolution. LROC's Narrow Angle Camera has 2 m resolution in one band, targeted. *Chang'e-1*/CCD (Yue et al. 2007) might also aid "before/after" sequences. Lunar Orbiter images, resolving to $\sim$1 m, form excellent "before" data for many sites, for morphological changes e.g., cores of explosive events over 40 years.

The prime technique for detecting changes between epochs of similar images is image subtraction, standard in studying supernovae, microlensing and variable stars. This produces photon Poisson noise-limited performance (Tomaney & Crotts 1996) and is well-matched to CCD or CMOS imagers, which at 1-2 arcsec FWHM resolution cover the Moon with 10-20 Mpixels, readily available. One needs $\gtrsim$2 pixels FWHM, otherwise non-Poisson residuals dominate. Our group has automated TLP monitors on the summit of Cerro Tololo, Chile and at Rutherfurd Observatory in New York that produce regular lunar imaging (Crotts et al. 2009), often simultaneously. Each cover the Near Side at 0.6 arcsec/pixel with images processed in 10s. This is sufficient to time-sample nearly all reported TLPs (see Paper I) and produce residual images free of systematic errors at Poisson levels (Figure 6). [8]

Imaging monitors open several possibilities for TLP studies, with extensive, objective records of changes in lunar appearance, at sensitivity levels $\sim$10 times better than the human eye. An automated system can distinguish contrast changes of 1% or better, whereas the human eye is limited to $\gtrsim$10%. We will measure the frequency of TLPs soon enough; Paper

[8]Multiple monitors can image TLPs in different bands or polarizations. TLP polarimetric anomalies (Dollfus 2000) occur on uncertain timescales (0.01-1 d). Other polarimetric transients (Dzhapiashvili & Ksanfomaliti 1962, Lipsky & Pospergelis 1966) are less constrained temporally. These are likely scattering linear polarizations; one can align one monitor's polarizer E-vector parallel to the Sun-Moon direction on the sky, and a second perpendicular. Three or four can construct linear Stokes parameters conventionally. Also we plan a parallel video channel which dumps high-speed sequences to disk given a TLP alert trigger.

I indicates perhaps one TLP per month visible to a human observing at full duty cycle. TLP monitors open new potential to alert other observers, triggering LE imaging of an active area, or spectroscopy of non-thermal processes and the gas associated with TLPs.

4.1.2. Ground-Based Spectroscopic/Hyperspectral Observations

Spatially resolved spectroscopy can 1) elucidate TLP physics, including identification of gas released, or 2) probe quasi-permanent changes in TLP sites. We must find changes in a four-dimensional dataset: two spatial dimensions, wavelength, and time, too much to monitor for transients. Fortunately, TLP monitoring can alert to an event in under 1000s, and a larger telescope with a spectrograph can observe the target (within ∼300s).

Whereas "hyperspectral" imaging usually refers to resolving power $R = \lambda/\Delta\lambda \approx 50 - 100$, where $\Delta\lambda$ is the FWHM resolution, TLP emission might be much narrower, thereby diluted at low resolution. For line emission, rejecting photons beyond the line profile yields contrasts up to 10^4 times better than the human eye using a telescope. IR hydration band near 3.4 μm have substructure over ∼20 nm, requiring $R \gtrsim 300$, compared to the IR SpeX on the NASA Infrared Telescope Facility with $R \lesssim 2000$. The 950 nm and 1.9 μm pyroxene bands show compositional shifts (Hazen, Bell & Mao 1978) seen at $R \approx 100$. Differentiating pyroxenes from Fe-bearing glass (Farr et al. 1980) requires $R \approx 50$. Observations involve scanning across the lunar face with a long slit spectrograph (Figure 7a). Since lunar surface spectral reflectance is homogenized by impact mixing, >99% of the light in such a spectrum is "subtracted away" by imposing this average spectrum and looking for deviations (Figure 7b). The data cube can be sliced in any wavelength to construct maps of lunar features in various bands. Figure 8 shows that surface features are reconstructed in detail and fidelity.

What narrow lines might we search for? The emission measure of gas in our model excited by solar radiation is undetectable except for the first few seconds. Coronal discharge offers a caveat. Reddish discharge may indicate Hα from dissociation of many possible molecules.[9] Rather than relying on Hα plus faint optical lines/bands to distinguish molecules, note that near-IR vibrational/rotational bands are brighter and more discriminatory.

[9]Kozyrev (1963) reported transient H_2 emission from Aristarchus (absent Balmer lines), and transient C_2 Swan bands (Kozyrev 1958). We do not advance a model to explain these observations.

4.1.3. Surface and Subsurface Radar

As in §3, internal water vapor might have produced ice in the regolith $\lesssim$15m subsurface, a venue for ground-penetrating radar, from lunar orbit. While epithermal neutrons and gamma radiation can detect hydrogen, they cannot penetrate $\gtrsim$1 m. Near the poles or subject to chemical modification (§3.3), ice might range closer to the surface. Past and current lunar radar include *Apollo 17*'s Lunar Sounder Experiment (LSE) (Brown 1972, Porcello 1974) at 5, 16 and 260 MHz, *Kaguya*'s Lunar Radar Sounder (Ono & Oya 2000) at 5 MHz (optionally, 1 MHz or 15 MHz), *LRO*'s Mini-RF (Mini Radio-Frequency Technology Demonstration) at 3 and ∼10 GHz, and Mini-SAR on *Chandrayaan-1* at 3 GHz (Bussey et al. 2006). Shorter wavelength radar could map possible changes in surface features in explosive outgassing, over tens of meters, in before/after radar sequences meshed with optical monitoring e.g., with *LRO* Mini-RF (Chin et al. 2007). For regolith and shallow bedrock, we need ∼100-300 MHz; LSE operated only a few orbits and near the equator. Near Side maps at ∼1 km resolution at 430 GHz (Campbell et al. 2007) could improve with intensive ground-based programs, or from lunar orbit, penetrating ∼ 20 m. Orbital missions can combine different frequencies and/or reception angles to improve spatial resolution and ground clutter, and reduce interference speckle noise. Earth-based radar maps exist at 40, 430 and 800 MHz (Thompson & Campbell 2005), also 2.3 GHz (Stacy 1993, Campbell et al. 2006a, b). Angles of incidence from Earth are large e.g., ∼ 60°, with echoes dominated by diffuse scattering not easily modulated. Circular polarization return can probe for surface water ice (Nozette 1996, 2001) but is questioned (Simpson 1998, Campbell et al. 2006a). Applying these to subsurface ice is at least as problematic, especially at ∼300 MHz to penetrate ∼15 m.

Finding subsurface ice is challenging. The dielectric constant is $K \approx 3$ for regolith, water ice (slightly higher), and many relevant powders of comparable specific gravity e.g., anorthosite and various basalts. These have attenuation lengths similar to ice, as well. Using net radar return alone, it will be difficult to distinguish ice from regolith. In terrestrial situations massive ice bodies reflect little internally (Moorman, Robinson & Burgess 2003). Ice-bearing regions should be relatively dark in radar images, if lunar ice-infused volumes homogenize or "anneal," either forming a uniform slab or by binding together regolith with ice in a uniform K bulk. On the other hand, hydrated regolith has K much higher than unhydrated (up to 10 times), and attenuation lengths over 10 times shorter (Chung 1972). Hydration effects are largest at lower frequencies, even below 100 MHz. If water ice perturbs regolith chemistry, increasing charge mobility as in a solution, K and conductivity increase, raising the loss tangent (conductivity divided by K and frequency). This high-K zone should cause reflections, depending strongly on the suddenness of the transition interface.

The 430 MHz radar map (Ghent et al. 2004) of Aristarchus and vicinity, site of ∼50% of

TLP and radon reports shows the 43-km diameter crater surrounded by low radar-reflectivity some 150 km across, especially downhill from the Aristarchus Plateau, which is dark to radar, except bright craters and Vallis Schröteri. The darker radar halo centered on Aristarchus itself is uniquely smooth, indicating that it was probably formed or modified by the impact, a few hundred My ago. This darkness might be interpreted as high loss tangent, as above, or simply fewer scatterers (Ghent et al. 2004) i.e., rocks of ∼1m size; it is undemonstrated why the latter applies in the ejecta blanket within the bright radar halo within 70 km of the Aristarchus center. Other craters, some as large as Aristarchus, have dark radar haloes, but none so extended (Ghent et al. 2005). The Aristarchus region matches subsurface ice redistributed by impact melt: dark, smooth radar-return centered on the impact (although tending downslope). One should search for dark radar areas around likely outgassing sites.

4.1.4. Monitoring from Low Lunar Orbit

Alpha-Particle Spectrometry: A ^{222}Rn atom random walks only ∼200 km before decaying (or sticking to a cold surface). In under a day, ^{222}Rn dispersal makes superfluous placing detectors <100 km above the surface (excepting r^{-2} sensitivity considerations). Alpha-particle spectrometers observed the Moon successfully for short times. The latitude coverage was limited on *Apollo 15* ($\mid Lat \mid \lesssim 26^\circ$ for 145 hours) and *Apollo 16* ($\mid Lat \mid \lesssim 5^\circ$, 128 h). *Lunar Prospector's* Alpha Particle Spectrometer (covering the entire Moon over 229 days spanning 16 months) was partially damaged and suffered sensitivity drops due to solar activity (Binder 1998). *Kaguya*'s Alpha Ray Detector (ARD) promised 25 times more sensitivity than Apollo (Nishimura et al. 2006), but sharing a failed power supply it has yet to produce results. *Apollo 15* observed outgassing events from Aristarchus and Grimaldi, *Apollo 16* none, and *Lunar Prospector* Aristarchus and Kepler integrated over the mission. Apollo and *Lunar Prospector* detected decay product ^{210}Po at mare/highlands boundaries from ^{222}Rn leakage over the past ∼100 y. An expected detection rate might be grossly estimated, consistent with an event 1-2 times per month detectable by *Apollo 15*, and by *Lunar Prospector* over the mission, with Aristarchus responsible for ∼50%. A polar orbiting alpha-particle spectrometer with a lifetime of a year or more and instantaneous sensitivity equal to Apollo's could produce a detailed map of outgassing on the lunar surface separate from optical manifestation. Two in polar orbit could cover the lunar surface every 1.8 half-lives of ^{222}Rn, nearly doubling sensitivity. Sensitivity can be increased if detectors incorporate solar wind vetos, or operate during solar minimum, and if detectors orient towards the lunar surface.

On-Orbit Mass Spectrometry: Unlike ^{222}Rn and its long surface residence, other outgassing events call for several instruments for efficient localization e.g., by mass spectrometry. With outgassing of hundreds of tons and tens of events per year, particle mass fluence from one

outburst seen 1000 km away approaches 10^{12} AMU cm^{-2}. A burst that is seen by a few detectors could be well constrained. Gas scale heights ∼100 km imply detectors near the ground. Conversely, an instantaneous outburst seen 100 km away will disperse less than one minute in arrival; detectors must operate rapidly. This was a problem e.g., the *Apollo 15* Orbital Mass Spectrometer Experiment (Hoffman & Hodges 1972) requiring 62s to scan through a factor of 2.3 in mass. Clearly there are two separate modes of gas propagation above the surface, neutral and ionized (Vondrak, Freeman & Lindeman 1974, Hodges et al. 1972), at rates of one to hundreds of tonne y^{-1} for each.

Operational strategies of these detectors are paramount. Consider an event 1000 km away, which will spread ∼ 500s in arrival time. A simple gas pressure gauge is too insensitive; with an ambient atmosphere not atypical e.g., number density $n \approx 10^4 - 10^5$ cm^{-3} (varying day/night e.g., Hodges, Hoffman & Johnson 2000), the collisonal background rate in 500 s amounts to 10× or more than the fluence for a typical outburst (assuming ∼ 20 AMU particles). Since interplanetary solar proton densities can vary by order unity in an hour or less (e.g., McGuire 2006), pressure alone is insufficient. Mass spectrometry subdivides incoming flux in mass, but also in direction, decreasing effective background rates.

One satellite particle detector cannot distinguish episodic behavior of outgassing versus spacecraft motion at ∼ 1.7 km s^{-1}. Localizing such signals between two platforms is ideal, at least for neutral species, if they constrain temporal/spatial location of specific outbursts using timing and signal strength differences. A timing difference indicates the distance difference to the source, with the source confined to a hyperboloid locus. Location on this hyperboloid is fixed by signal strengths, plus left/right ambiguity from detector directionality. A mean nearest satellite distance of 1000 km from arbitrary sources requires $\gtrsim$10 low orbital platforms. Mass spectrometers on the surface can maintain such density over smaller areas efficiently once we know roughly where sources may be. A mass spectrometer planned for *Lunar Atmospheric and Dust Environment Explorer* (*LADEE*) sits on one platform in equatorial orbit; geographical resolution of outgassing events will be poor.[10]

[10] "Low maintenance" lunar orbits at low altitude require few corrections due to mascon, but must maintain "frozen orbit" inclination angles i =27, 50, 76 or 86° (e.g., Ramanan & Adimurthy 2005). If we want to maintain a position over the terminator (sun-synchronous orbit), we requires a precession rate $\omega_p = 0.99°d^{-1} = 2 \times 10^{-7}$ rad s^{-1}. Alternatively, LADEE achieves this by a precessing, highly eccentric orbit, but spends a small fracton of its time near the lunar surface. Precession is fixed by coefficient $J_2 = (2.034 \pm 0.001) \times 10^{-4}$ (Konopliv et al. 1998) according to $\omega_p = -(3a^2 J_2 \sqrt{GM} cos\ i)/(2r^{7/2})$, where a is lunar radius, ω orbital angular speed, M lunar mass and r orbital radius. Precession due to the Sun and Earth are much smaller. One cannot effectively institute both sun synchronicity in a polar orbit, however, since the maximum inclination orbit with $\omega_p = 2 \times 10^{-7}$ s^{-1} occurs at 47° (or else below the surface). To force sun-synchronicity at $i = 86°$, $\omega_p = 1.5 \times 10^{-8}$ s^{-1}, requires only $a = 0.3$ mm s^{-2} which could even be accomplished by a Hall-effect ion engine or even a solar sail (with 330 cm^2 g^{-1}).

4.1.5. In-Situ and Near Surface Exploration

Surveying *in situ* approaches to studying volatiles is beyond the scope of this paper;[11] we emphasize a few key points. The key effort is to focus from wide-ranging reconnaissance down to scales where lunar volatiles can be sampled near their source. Primary global strategies are optical transient monitoring (Near Side, resolution ∼1 km) and orbital ^{222}Rn and 3μm detection (both hemispheres, ∼100 km and <1 km, respectively). Even trusting that TLPs trace volatiles and centroiding TLPs to 10% of a resolution element, localization error (∼100 m) could preclude easy *in situ* followup. (In Appendix I we outline improving this to ∼ 10 m.) Two simple *in situ* technologies could isolate outgassing sources below 100 km scales. First, three alpha particle detectors on the surface can triangulate nearby ^{222}Rn outgassing sources, using strength and time delay in arrival of random walking ^{222}Rn. Secondly, a mass spectrometer that can reconstruct the ballistic trajectory of neutrals from the source (Austin et al. 2008, Daly, Radebaugh & Austin 2009) can construct an "image" of transient outgassing sources over regions up to 1000 km across. This spectrometer is not overwhelmed by pulsed sources while measuring masses over a wide range. Further technologies could pinpoint subsurface structure at 10 m scales from information at 1 km.[12]

By LACE's deployment with the final Apollo landing, the outgassing environment was contaminated by anthropogenic gas (Freeman & Hills 1991) especially near landing sites; each mission of human exploration will deliver tens of tonnes gases to the surface, with species relevant to endogenous volcanic gas, approaching or exceeding the annual endogenous output of such gases.[13] Depending on spacecraft orientations and trajectories when thrusting, they may deliver ∼20 tonnes of mostly water to the surface, which will remain up to about one lunation, making suspect measurements of these and other species for years.

---

[11]Our research group, AEOLUS: "Atmosphere seen from Earth, Orbit and the LUnar Surface," is developing ways to efficiently transfer information from remote sensing to *in situ* research of lunar volatiles.

[12]These include local seismic arrays, local ground penetrating radar, magnetometer and infrared laser arrays. The latter would consist of lasers, mirrors and sensors on towers for specific molecular species, either constructed to exploit a specific species e.g., CO_2, or tuned to one of several species' vibrational-rotational states. On smaller scales (1-100 m) several varieties of mass spectroscopy might prove effective, including downward-sniffing spectrometers, triangulating outburst detectors arrays, and pyrolysis mass spectrometers (ten Kate et al. 2009) which heat regolith samples in search of absorbed species from previous outgassing.

[13]Constellation spacecraft Orion burn N_2O_4 (nitrogen teroxide) and $CH_3N_2H_3$ (mono-methyl hydrazine), with Altair propelled by liquid oxygen and hydrogen. Future missions might use liquid O_2 and CH_4. Earth Departure Stages might deliver residual O_2 and H_2 in lunar impact. Altair (and EDS) produce water, and Orion exhausts H_2O, CO_2 and N_2. N_2 was the prime candidate constituent in an outburst seen by the *Apollo 15* over Mare Orientale: Hoffman & Hodges 1972, perhaps anthropogenically - Hodges 1991.

5. Discussion and Conclusions

The origin of TLPs has been mysterious, and their correlation to outgassing, while strong, was only circumstantial. The plausible generation of TLP-like events as simple consequence of outgassing from the interior lends credence to a possible causal link. We present a model tied to outgassing from deep below the regolith that reproduces the time and spatial scale of reported TLPs, suggesting a causal link to outgassing. Radiogenic gas evolved from the regolith cannot provide the concentration to produce a noticeable explosive event.

Apollo and later data were insufficiently sensitive to establish the level of outgassing beyond ^{222}Rn, and isotopes of Ar, plus He, presumably, and did detect marginally molecular gas, but of uncertain origin, particularly CH_4, Reviewing the evidence and available techniques, there are several gases that should be highlighted as crucial outgassing tracers. ^{222}Rn (and its products e.g., ^{210}Po) can be detected remotely of course and are unique in terms of their mapping potential, while being a minor fraction of escaping gas, presumably. ^{40}Ar is a major mass constituent of the atmosphere and unlike ^{4}He is not confused with the solar wind. Both ^{222}Rn and ^{40}Ar will favor KREEP terrane in the western maria, presumably.

If outgassing arises in the deep interior, one cannot neglect indications that at one time this was dominated by volcanic, molecular gas. Particular among these is water vapor, passing its triple point temperature in rising through the regolith. Given a high enough concentration, therefore, one should expect the production of water ice. The conditions under the regolith, particularly near the lunar poles, are favorable for such ice to persist even over geological time interval. It is possible that ice generated there when outgassing was more active still remains. We further point out that the plausible chemical interaction of such molecular gases with the regolith is the production of cement-like compounds that might radically alter the diffusivity of the regolith. Given the temperature evolution of the regolith, this non-diffusive layer would isolate the volatile outflow from the vacuum.

The question remains how we will detect such molecular outgassing effects, given their largely covert nature; this is greatly complicated by possible anthropogenic contamination in the future. Among molecular gases, sulfur e.g., SO_2 is the predominate volatile detected in deep-interior fire fountain glasses, a key factor in deciding what to pursue as a volcanic tracer. Furthermore, essential no liquid or hybrid rocket propellant candidate contain sulfur, and the only sulfuric solid propellants are fairly outdated e.g., black powder and Zn-S. NASA and hopefully other space agencies have no plans to use these on lunar missions.

Despite the hypotheses and methods outlined above, there is great doubt regarding the nature of lunar outgassing. Water is of obvious and diverse interest, and CO_2 and CO, while missing as apparent constituents, are interesting as drivers for fire fountain eruption.

Plausibly the only way to study these components reliably is before the new introduction of large spacecraft into the lunar environment. Given uncertainty of how these gases and SO_2 might interact with the regolith, this early study appears paramount.

Significantly, many years to come monitoring for optical transients will be best done from Earth's surface, even considering the important contributions that will be made by lunar spacecraft probes in the near future. However, these spacecraft will be very useful in evaluating the nature of transient events in synergy with ground-based monitoring. Given the likely behavior of outgassing events, it is unclear that in-situ efforts alone will necessarily isolate their sources within significant winnowing of the field by remote sensing. Early placement of capable mass spectrometers of the lunar surface, however, might prove very useful in refining our knowledge of outgassing composition, in particular a dominant component that could be used as a tracer to monitor outgassing activity with more simple detectors. This should take place before significant atmospheric pollution by large spacecraft, which will produce many candidate tracer gases in their exhaust.

Finally, as we edit this paper's final version, several works have become available indicating confirmed lunar regolith hydration signals (Pieters et al. 2009, Clark 2009, Sunshine et al. 2009) in the 3μm band, and we comments about these here. These show a strong increase in hydration signal towards the poles, as predicted in §4. To our knowledge our model is uniquely consistent with this and the general hydration signal strength, in places $\gtrsim$700 ppm by mass (also with Vilas et al. 1999, 2008). Unfortunately the Moon Mineralogy Mapper (M^3: Pieters et al. 2006), in finding this signal, but not completely mapping it, provided tentative indication of its large scale distribution varying over a lunation. This variation can be studied from Earth with a simple near/mid IR camera (InSb or red-extended HgCdTe) with on- and off-band filters for IR hydration bands (or 0.7μm: Vilas et al. 1999). To complete this valuable work, along with other instruments needing a lunar polar orbiter (alpha-particle spectrometer, ground-penetrating radar, mass spectrometers, etc.), an instrument similar to M^3 should probably fly again before human lunar missions. Note that the same type and level of signal was detected by *Luna 24* (Akhmanova et al. 1978), and these authors believed it not due to terrestrial contamination. They detected increasing hydration with depth into the regolith, a likely circumstance in our model. This core sample reached 2 meters depth, several times deeper than epithermal neutrons e.g., seen on *Lunar Prospector* or *LRO*, and corresponding to an impact gardening over $\sim$2 G.y. Such a gradient arises naturally from seepage of water vapor, but water and/or hydroxyl from solar wind proton implantation may not explain the concentration of 3μm signal to the poles and the *Luna 24* hydration depth profile. This offers a challenge for this model, or for water delivered by comets and/or meteoroids. In a separate paper we will review further evidence supporting endogenous origin of lunar hydration.

Acknowledgements

We would much like to thank Alan Binder and James Applegate, as well as Daniel Savin, Daniel Austin, Ed Spiegel and the other members of AEOLUS ("Atmosphere as seen from, Earth, Orbit and LUnar Orbit") for helpful discussion. This research was supported in part by NASA (07-PAST07-0028 and 07-LASER07-0005), the National Geographic Society (CRE Grant 8304-07), and Columbia University.

Appendix I: Imaging from High Orbit:

Given constraints on imaging from Earth, we consider imaging monitors closer to the Moon. We propose no special-purpose missions, but detectors that could ride on other platforms e.g., does lunar exploration require communications with line-of-sight access to all points on the Moon's surface (except within deep craters, etc.)? This might also serve for comprehensive imaging monitoring. A minimal full network has a tetrahedral geometry with points ∼60000 km above the surface: a single platform at Earth-Moon Lagrange point L1, covering most of the Near Side, and three points in wide halo orbits around L2 for the Far Side plus limb seen from Earth. Proposals exist for an L1 orbital transfer facility (Lo 2004, Ross 2006). No single satellite sees the entire Far Side, especially since farside radio astronomy might restrict low-frequency transmission i.e., lasers only. One L2 satellite covers $\lesssim$97% of the Far Side (subtending 176°.8, selenocentrically); full coverage (plus some redundancy) requires three satellites (plus L1). With this configuration, the farthest point from a satellite will be typically 71° (selenocentrically), foreshortened by ~ 3 times. Such an imaging monitor might be ambitious; to achieve 100m FWHM at the lunar sub-satellite point requires ∼4 Gpixels, aperture $\gtrsim 0.5$ m, and field-of-view 3°.3. Each such monitor on an existing platform will cost perhaps $100M. In the meantime, we should accomplish what we can from the ground.

References:

Adams, J.B. 1974, JGR, 79, 4829.

Adorjan, A.S. 1970, J. Spacecraft & Rockets, 7, 378.

Akhmanova, M.V., Dement'yev, B.V. & Markov, M.N. 1978, Geokhimiya, 2, 285.

Akhmanova, M.V., Dement'yev, B.V., Markov, M.N. & Sushchinskii, M.M. 1972, Cosmic Res., 10, 381

Allen, C.C., et al. 1998, Lun. Plan. Sci. Conf., 29, 1690.

Anders, E. 1970, Science, 169, 1309.

Anders, E. Ganapathy, R., Krähenbühl, U. & Morgan, J.W. 1973, The Moon, 8, 3.

Anderson, R.. et al. 1965, Science, 148, 1179.

Andreas 2007, Icarus, 286, 24.

Austin, D.E., Miller, I., Daly, T., Crotts, A., Syrstad, E., Brinckerhoff, W. & Radebaugh, J. 2008, NLSI Lun. Sci. Conf., 2074.

Bart, G.D. & Melosh, H.J. 2005, D.P.S., 57, 57.07.

Bautsch, M., Varadinek, P., Wege, S. & Niedrig, H. 1994, J. Vac. Sci. Technol. A., 12, 591.

Basu, A. & Molinaroli, E. 2001, Earth Moon & Plan., 85, 25.

Brantley, S.L. 2004, in "Treatise on Geochemistry" eds. H.D. Holland & K.K. Turekian (Elsevier: Amsterdam), section 5.03.

Brown, W.E., Jr. 1972, Earth Moon Plan., 4, 133.

Buratti, B.J., McConnochie, T.H., Calkins, S.B., Hillier, J.K. & Herkenhoff, K.E. 2000, Icarus, 146, 98.

Bussey, B., Spudis, P.D., Lichtenberg, C., Marinelli, B. & Nozette, S. 2006, in *LCROSS Selection Conf.*, (LPI: Houston), 9013.

Cameron, W.S. 1972, Icarus, 16, 339.

Cameron, W.S. 1977, Phys. Earth Planet. Inter., 14, 194.

Campbell, B.A., Campbell, D.B., Margot, J.-L., Ghent, R.R., Nolan, M., Carter, L.M., Stacy, N.J.S. 2007, Eos, 88, 13.

Campbell, D.B., Campbell, B.A., Carter, L.M., Margot, J.-L. & Stacy, N.J.S. 2006a, Nature,

443, 835.

Campbell, B.A., Carter, L.M., Campbell, D.B., Hawke, B.R., Ghent, R.R. & Margot, J.-L. 2006b, Lun. Plan. Sci. Conf., 37, 1717.

Carbognani, A. 2004, Astronomia, 5, 12.

Carrier, W.D., Olhoeft, G.R. & Mendell, W. 1991, in "Lunar Sourcebook," eds. G.H. Heiken, D.T. Vaniman & B.M. French (Cambridge U.: Cambridge), p. 475.

Charette, M.P., Adams, J.B., Soderblom, L.A., Gaffey, M.J. & McCord, T.B. 1976, Lun. Sci. Conf., 7, 2579.

Charles, R.W., Hewitt, D.A. & Wones, D.R. 1971, Lun. Sci. Conf., 1, 645.

Chevrier, V., et al. 2007, GRL, 34, L02203.

Chin, G., et al. 2007, Lun. Plan. Sci. Conf., 38, 1764.

Chung, D.H. 1972, Earth Moon & Plan., 4, 356.

Clark, R.N. 2009, Science Express Rep., 10.1126/science.1178105.

Cocks, F.H., et al. 2002, Icarus, 160, 386.

Collins, G.S. 2001, Lun. Plan. Sci. Conf., 32, 1752.

Compton, K.T., Lilly, E.G. & Olmstead, P.S. 1920, Phys. Rev., 16, 282.

Crotts et al. 2009, in preparation.

Crotts, A.P.S. 2008, ApJ, 687, 1186.

Crotts, A.P.S. 2009, ApJ, 697, 1.

Cullingford, H.S. & Keller, M.D. 1988, in *2nd Conf. on Lunar Bases and Space Activities*, ed. W.W. Mendell, NASA Conf. Pub. 3166, p. 497.

Daly, T., Radebaugh, J. & Austin, D.E. 2009, Lun. Plan. Sci. Conf., 40, 2411.

Davis, S.S. 2009, Icarus, 202, 383.

Dollfus, A. 2000, Icarus, 146, 430.

Drake, M.J. & Stimpfl, M. 2007, Lun. Plan. Sci. Conf., 38, 1179.

Dzhapiashvili, V.P. & Ksanfomaliti, L.V. 1962, The Moon, IAU Symp. 14, (Academic Press: London), p. 463.

Elkins-Tanton, L.T., Chatterjee, N. & Grove, T.L. 2003, Meteor. & Plan. Sci., 38, 515.

Epstein, S. & Taylor, H.P., Jr. 1972, Geochim. Cosmochim. Acta, 36 (Suppl. 3), 1429.

Farmer, C.B. 1976, Icarus, 28, 279.

Farr, T.G., Bates, B., Ralph, R.L. & Adams, J.B. 1980, Lun. Plan. Sci., 11, 276.

Feynmann, R.P. 1974, Engineer. & Sci., 37, 7.

Freeman, J.W., Jr. & Hills, H.K. 1991, GRL, 18, 2109.

Fried, D.L. 1978, Opt. Soc. Am. J., 68, 1651.

Friedman, B., Saal, A.E., Hauri, E.H., van Orman, J.A. & Rutherford, M.J. 2009, Lun. Plan. Sci. Conf., 40, 2444.

Friesen, L.J. 1975, The Moon, 13, 425.

Gammage, R.B. & Holmes, H.F. 1975, Lun. Sci. Conf., 6, 3305.

Garlick, G.F.J., Steigmann, G.A. & Lamb, W.E. 1972a, Nature, 238, 13.

Garlick, G.F.J., Steigmann, G.A., Lamb, W.E. & Geake, J.E. 1972b, 1972, Lun. Plan. Sci. Conf., 3, 2681.

Garvin, J., Robinson, M., Skillman, D., Pieters, C., Hapke, B. & Ulmer, M. 2005, *HST* Proposal GO 10719.

Gault, D.E., Hörz, F, Brownlee, D.E. & Hartung, J.B. 1974, Lun. Plan. Sci. Conf., 5, 260.

Geake, J.E. & Mills, A.A. 1977, Phys. Earth Planet. Inter., 14, 299.

Gerlach, T.M. & Graeber, E.J. 1985, Nature, 313, 274

Ghent, R.R., Leverington, D.K., Campbell, B.A., Hawke, B.R. & Campbell, D.B. 2004, Lun. Plan. Sci. Conf., 35, 1679.

Ghent, R.R., Leverington, D.K., Campbell, B.A., Hawke, B.R. & Campbell, D.B. 2005, JGR. 110, doi: 10.1029/2004JE002366.

Gibson, E.K. & Moore, G.W. 1973, Science, 179, 69.

Haynes, D.R., Tro, N.J. & George, S.M. 1992, J. Phys. Chem., 96, 8502.

Hazen, R.M., Bell, P.M. & Mao, H.K. 1978, Lun. Plan. Sci., 9, 483.

Hodges, R.R., Jr. 1977, Phys. Earth & Planet. Inter., 14, 282.

Hodges, R.R., Jr. 1980, Proc. Lun. Plan. Sci. Conf., 11, 2463.

Hodges, R.R., Jr. 1991, *personnel communication*, in Stern, A. 1999, Rev. Geophys., 37, 4.

Hodges, R.R., Jr., Hoffman, J.H., Yeh, T.T.J. & Chang, G.K. 1972, JGR, 77, 4079

Hodges, R.R., Jr., Hoffman, J.H., Johnson, F.S. & Evans, D.E. 1973, Lun. Sci. Conf., 4, 2855.

Hodges, R.R., Jr., Hoffman, J.H. & Johnson, F.S. 1974, Icarus, 21, 415.

Hodges, R.R., Jr. & Hoffman, J.H. 1975, Lun. Plan. Sci. Conf., 6, 3039.

Hoffman, J.H. & Hodges, R.R., Jr. 1975, Moon, 14, 159.

Horiguchi, T., Saeki, N., Yoneda, T., Hoshi, T. & Lin, T.D. 1996, in "Space V: 5th Internat'l Conf. Engin., Constr. & Operat. in Space," ed. S.W. Stewart, ASCE Proc., 207, 86.

Horiguchi, T., Saeki, N., Yoneda, T., Hoshi, T. & Lin, T.D. 1998, in "Space '98: 6th Internat'l Conf. Engin., Constr. & Operat. in Space," eds. R.G. Galloway & S.L. Lokaj, ASCE Proc., 206, 65.

Hughes, D.W. 1980, Nature, 285, 438.

Ingersoll, A.P. 1970, Science, 168, 972.

Kanamori, H. in *Concrete Under Severe Conditions 1: Environment and Loading*, eds. K. Sakai, N. Banthia & O.E. Gjorv (Chapman & Hall: London), p. 1283.

Kozyrev, N.A. 1958, Sov. Intern't'l Geop. Yr. Bull., PB 13162-42 (see also 1962, in *The Moon, IAU Symp. 14*, eds. Z. Kopal & Z.K. Mikhailov (Academic: New York), p. 263.

Kozyrev, N.A. 1963, Nature, 198, 979.

Krähenbühl, U., Ganapathy, R., Morgan, J.W. & Anders, E. 1973, Science, 180, 858.

Langseth, M.G., Jr., Clarke, S.P., Jr., Chute, J.L., Jr., Keihm, S.J. & Wechsler, A.E. 1972, in *Apollo 15 Preliminary Science Report*, NASA SP-289, p. 11-1.

Langseth, M.G., Jr., Keihm, S.J. & Chute, J.L., Jr. 1973, in *Apollo 17 Preliminary Science Report*, NASA SP-330, p. 9-1.

Langseth, M.G. & Keihm, S.J. 1977, in *Soviet-American Conference on Geochemistry of the Moon and Planets*, NASA SP-370, p. 283.

Law, N.M., Mackay, C.D. & Baldwin, J.E. 2006, A&A, 446, 739.

Lebofsky, L.A., Feierberg, M.A., Tokunaga, A.T., Larson, H.P. & Johnson, J.R. 1981, Icarus, 48, 453

Lipsky, Yu.N. & Pospergelis, M.M. 1966, Astronomicheskii Tsirkular, 389, 1.

Lo, M.W. 2004, in "Proc. Internat'l Lunar Conf. 2003, ILEWG 5" (Adv. in Astronaut. Sci., Sci. & Tech. Ser., Vol. 108), eds. S.M. Durst et al. (Univelt: San Diego), p. 214.

Lucey, P.G., Blewett, D.T., Taylor, G.J. & Hawke, B.R. 2000, JGR, 105, 20377.

Lucey, P.G., Taylor, G.J. & Hawke, B.R. 1998, Lun. Plan. Sci. Conf., 29, 1356.

Lunine, J., Graps, A., O'Brien, D.P., Morbidelli, A., Leshin, L. & Coradini, A. 2007, Lun. Plan. Sci. Conf., 28, 1616.

Markov, M.N., Petrov, V.S., Akhmanova, M.V. & Dementev, B.V. 1979, in *Space Research, Proc. Open Mtgs. Working Groups* (Pergamon: Oxford), p. 189.

Martin, R.T., Winkler, J.L., Johnson S.W. & Carrier, III, W.D. 1973, "Measurement of conductance of Apollo 12 lunar simulant taken in the molecular flow range for helium, argon, and krypton gases." Unpublished report quoted in Carrier et al. (1991).

McCubbin, F.M., Nekvasil, H. & Lindsley, D.H. 2007, Lun. Plan. Sci. Conf., 38, 1354.

McEwen, A.S., Robinson, M.S., Eliason, E.M., Lucey, P.G., Duxbury, T.C. & Spudis, P.D. 1994, Science, 266, 1858.

McKay, D.S., Fruland, R.M. & Heiken, G.H. 1974, Lun. Plan. Sci. Conf., 5, 887.

McKay, D.S., et al. 1991, in "Lunar Sourcebook," eds. G.H. Heiken, D.T. Vaniman & B.M. French (Cambridge U. Press: Cambridge), p. 285.

Middlehurst, B.M. 1977, Roy. Soc. Phil. Trans. A, 285, 485.

Mills, A.A. 1969, Nature, 224, 863

Mills, A.A. 1970, Nature, 225, 939.

Moorman, B.J., Robinson, S.D. & Burgess, M.M. 2003, Permafrost & Periglac. Proc., 14, 319.

Morgan, T.H. & Shemansky, D.E. 1991, JGR, 96, 1351.

Mukherjee, N.R. 1975, The Moon, 14, 169.

Mukherjee, N.R. & Siscoe, G.L. 1973, JGR, 78, 1741.

Neukum, G., et al. 2001, Space & Sci. Rev., 96, 55.

Nishimura, J., et al. 2006, Adv. in Space Res., 37, 3.

Nozette, S. et al. 1996, Science, 274, 1495.

Nozette, S. et al. 2001, JGR, 106, 23253.

O'Hara, M.J. 2000, J. Petrology, 41, 11, 1545.

Ohtake, M. et al. 2007, Lun. Plan. Sci. Conf., 38, 1829.

Ono, T. & Oya, H. 2000, Earth Plan. Space, 52, 629.

Pearse, R.W.B. & Gaydon, A.G. 1963, *The Identification of Molecular Spectra*, (Ugsman & Hall: London)

Perel, J., Mahoney, J.F., Kalensher, B.E. & Forrester, A.T. 1981, Appl. Phys. Let., 38, 320.

Pieters, C.M., et al. 2005, http://moonmineralogymapper.jpl.nasa.gov/SCIENCE/Volatiles/

Pieters, C. et al. 2006, Lun. Plan. Sci. Conf., 37, 1630.

Pieters, C. et al. 2009, Science Express Rep., 10.1126/science.1178658.

Porcello, L.J, et al. 1974, Proc. IEEE, 62, 769.

Quaide, W. & Oberbeck, V. 1975, Moon, 13, 27.

Reader, J. & Corliss, C.H. 1980, CRC Handbook of Chemistry & Physics, 68.

Rivkin, A.S., Howell, E.S., Britt, D.T., Lebofsky, L.A., Nolan, M.C. Branston, D.D. 1995, Icarus, 117, 90

Rivkin et al. 2002, Asteroids III, 237

Robinson, J.H. 1986, JBAA, 97, 12.

Robinson, M.S. et al. 2005, Lun. Plan. Sci. Conf., 36, 1576.

Ross, S.D. 2006, Am. Sci., 94, 230.

Rubey, W.W. 1964, in "Origin & Evolution of Atmospheres & Oceans," eds. P.J. Brancazio & A.G.W. Cameron (Wiley: New York), p. 1.

Rutherford, M.J. & Papale, P. 2009, Geology, 37, 219.

Saito, Y., Tanaka, S., Takita, J., Horai, K. & Hagermann, A. 2007, Lun. Plan. Sci. Conf., 38, 2197.

Saal, A.E., Hauri, E.H., Cascio, M.L., van Orman, J.A., Rutherford, M.J. & Cooper, R.F. 2008, Nature, 454, 192.

Sato, M. 1976, Proc. Lun. & Plan. Sci. Conf., 7, 1323.

Sato, M. 1979, Proc. Lun. & Plan. Sci. Conf., 10, 311.

Schorghofer, N. & Taylor, G.J. 2007, JGR, 112, E02010.

Schultz, P.H., Staid, M.I. & Pieters, C.M. 2006, Nature, 444, 184.

Schumm, S.A. 1970, Geol. Soc. Amer. Bull., 81, 2539.

Shearer, C.K., Layne, G.D. & Papike, J.J. 1994, Geochim. CosmoChim. Acta, 58, 5349.

Siegal, B.S. & Gold, D.P. 1973, Moon, 6, 304.

Simpson, R.A. 1998, in "Workshop on New Views of the Moon," eds. B.L. Jolliff & G. Ryder (LPI: Houston), p. 61.

Speedy, R.J., Denebetti, P.G., Smith, R.S., Huang, C. & Kay, B.D. 1996, J. Chem. Phys., 105, 240.

Spohn, T, Konrad, W., Breuer, D. & Ziethe, R. 2001, Icarus, 149, 54.

Spudis, P.H. & Schultz, P.D. 1983, Nature, 302, 233.

Stacy, N.J.S. 1993, Ph.D. thesis (Cornell U.).

Stern, A. 1999, Rev. Geophys., 37, 4.

Stimpfl, M., de Leeuw, N.H., Drake, M.J. & Deymier, P. 2007, Lun. Plan. Sci. Conf., 38, 1183.

Stubbs, V.J., Vondrak, R.R. & Farrell, W.H. 2005, Lun. Plan. Sci. Conf., 36, 1899.

Sunshine, J.M. et al. 2009, Science Express Rep., 10.1126/science.1179788.

Taylor, S.R. 1975, *Lunar Science: a Post-Apollo View* (Pergamon: NY), 372 pp.

ten Kate, I.L., Glavin, D.P. & the VAPoR team, Lun. Plan. Sci. Conf., 40, 2232.

Thomas, G.E. 1974, Science, 183, 1197.

Thomas, R.J., et al. 2007, Science, 315, 1097.

Thompson, T.W. & Campbell, B.A. 2005, Lun. Plan. Sci. Conf., 36, 1535.

Tomaney, A. & Crotts, A.P.S. 1996, AJ, 112, 2872.

Tubbs, R.N. 2003, Ph.D. thesis (University of Cambridge).

Vilas, F., Dominque, D.L., Jensen, E.A., McFadden, L.A., Coombs, C.R. & Mendell, W.W. 1999, Lun. Plan. Sci. Conf., 30, 1343.

Vilas, F., Jensen, E.A., Dominque, D.L., McFadden, L.A., Runyon, C.J. & Mendell, W.W. 2008, Earth, Planets & Space, 60, 67.

Volquardsen, E.L., Rivkin, A.S. & Bus, S.J. 2004, DPS, 36, 32.13.

Vondrak, R.R., Freeman, J.W. & Lindeman, R.A. 1974, Lun. & Plan. Sci. Conf., 5, 2945.

Washburn, E., et al., eds. 2003, *International Critical Tables of Numerical Data, Physics, Chemistry and Technology* (Knovel: Norwich, NY), elec. edition.

Williams, R.J. & Gibson, E.K. 1972, Earth Plan. Sci. Let., 17, 84.

Wilson, L. & Head, J.W. 2003, Geophys. Res. Let., 30, 1605.

Yue, Z., Xie, H.. Liu, J. & Ouyang, Z. 2007, Lun. Plan. Sci. Conf., 38, 2082.

Zito, R.R. 1989, Icarus, 82, 419.

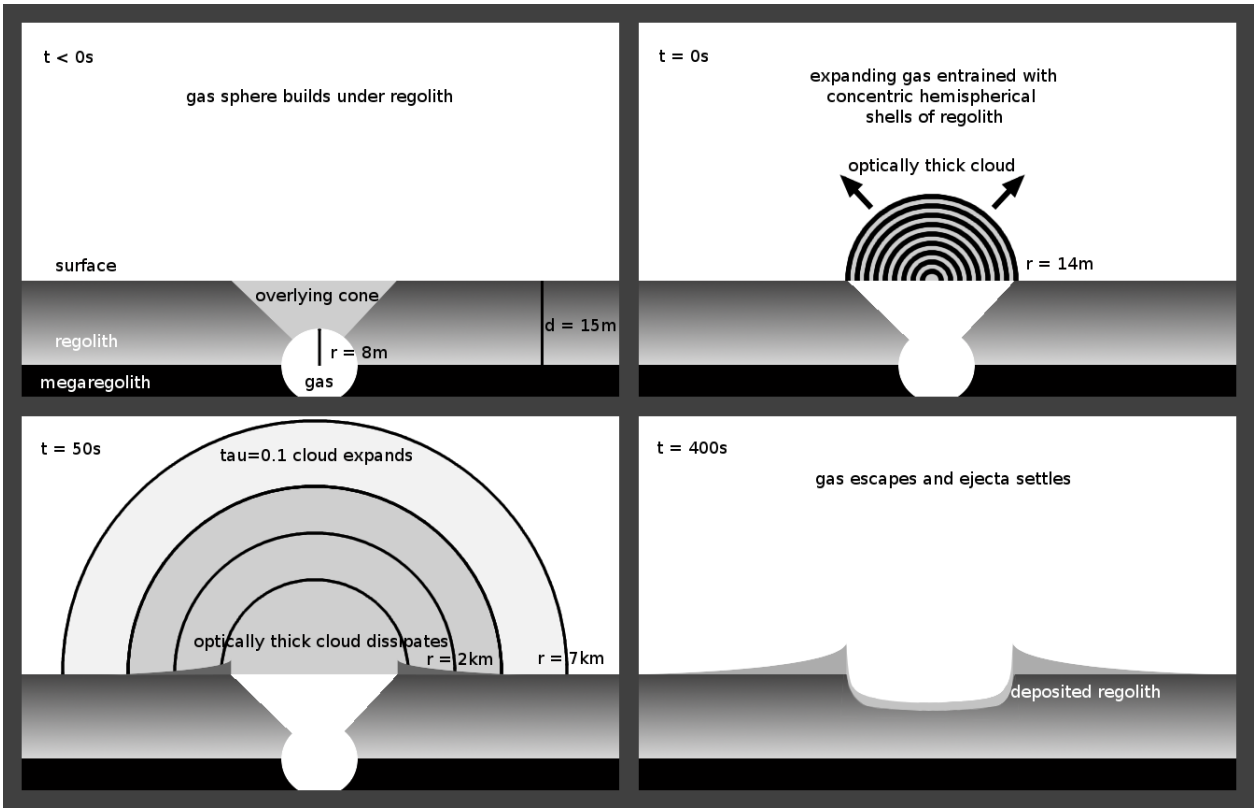

Fig. 1.— A sketch of our 1D spherically-symmetric model explosion. **Frame 1:** venting gas builds up at the interface between the megaregolith and the low-diffusivity regolith. It builds until its pressure is sufficient to lift the overlying cone of regolith to the surface. **Frame 2:** we assume that this regolith/gas mixture now translates into a hemispherical volume on the surface. This volume is uniform in gas density, but it is populated with concentric, hemispherical shells of regolith particles (represented as points 45 degrees up the side of each arc), each feeling a pressure from the expanding gas. As the cloud expands, the equations of motion are numerically integrated for each shell in the cloud according to its mass and regolith particle size composition. **Frame 3:** the cloud expands until it reaches a point where it is no longer optically thick as viewed from above, but the dust still entrained in the cloud continues to expand and a thinner component ($\tau = 0.1$) remains somewhat visible from above. Figure 2 shows the detailed evolution of these clouds. Regolith that has fallen out of the gas cloud begins to pile up on the ground around the crater. **Frame 4:** all of the gas has escaped and all entrained regolith is deposited on the ground around the crater in a manner shown in Figure 4.

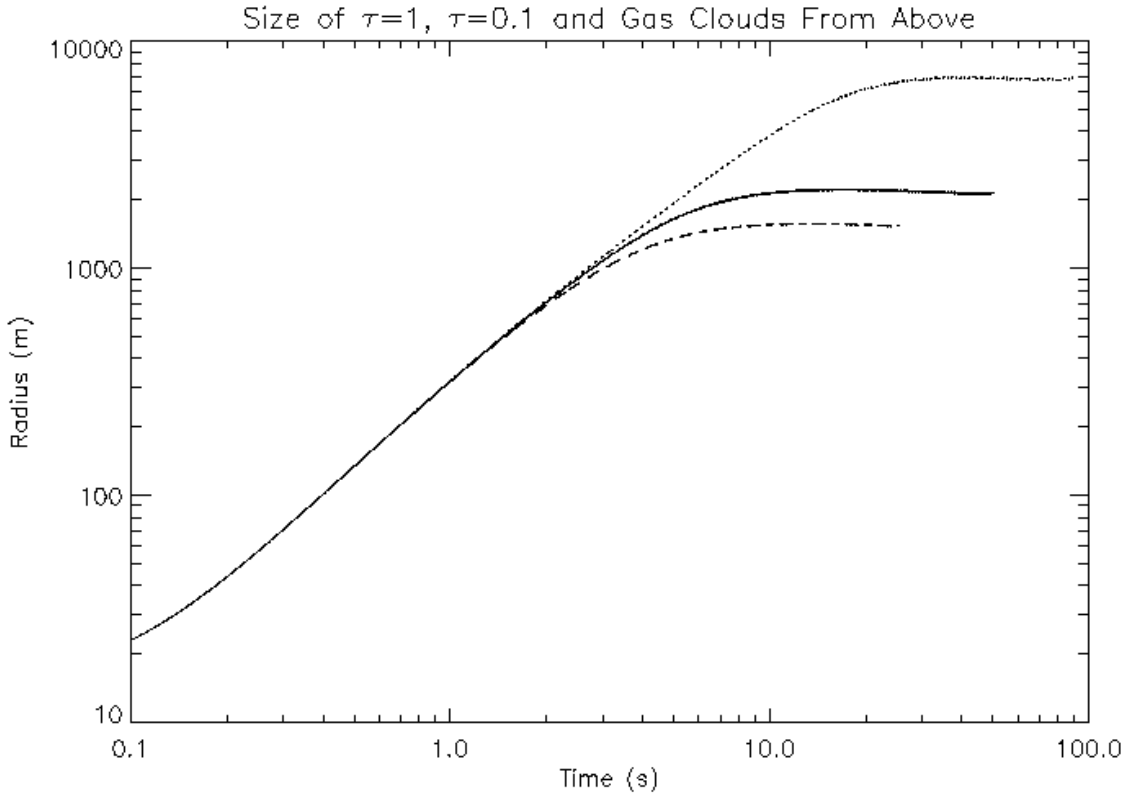

Fig. 2.— The size of the various components of the clouds as seen from above, versus time after the initial explosion, for a "minimal TLP." The solid line represents the radius of the dust cloud with optical thickness $\tau = 1$ as seen from above. The dotted line represents the radius of the dust cloud with $\tau = 0.1$ as seen from above. These two optical depth values correspond roughly to the level of change in contrast that might be considered easy versus marginal to detect with the human eye observing lunar surface features affected by the event. The dashed line represents the radius of the outermost layer of the gas cloud still constrained by the dust cloud. At 10 s after the explosion, the $\tau = 1$ portion of the cloud has expanded to 2 km radius and stops expanding; after 50 s no portion of the cloud remains with $\tau = 1$. After 90 s, the $\tau = 0.1$ portion of the cloud has also disappeared, having first expanded to 7 km in radius.

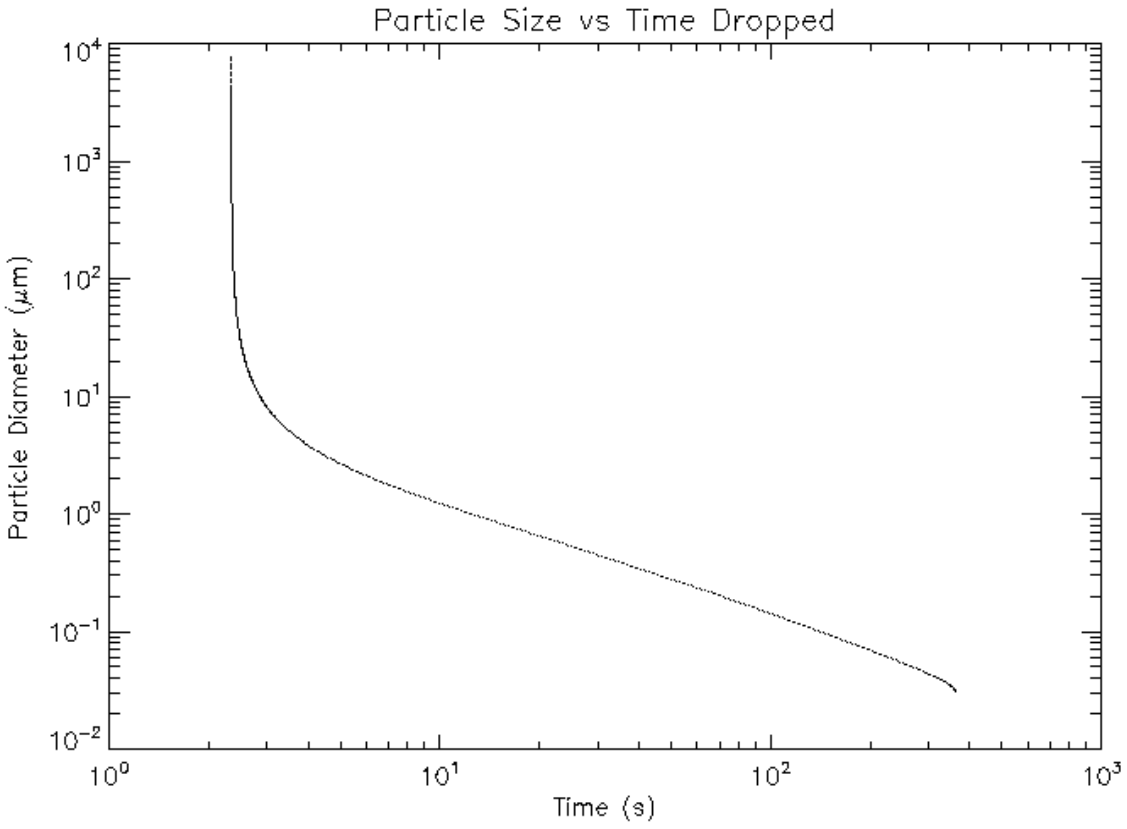

Fig. 3.— The time required for a typical regolith particle of the diameter shown to fall out of the expanding cloud back to the lunar surface. Particles larger than about 30 micron (slightly more than 50% by mass) rain immediately to the ground, whereas particles smaller than optical wavelength remain aloft for at least several minutes.

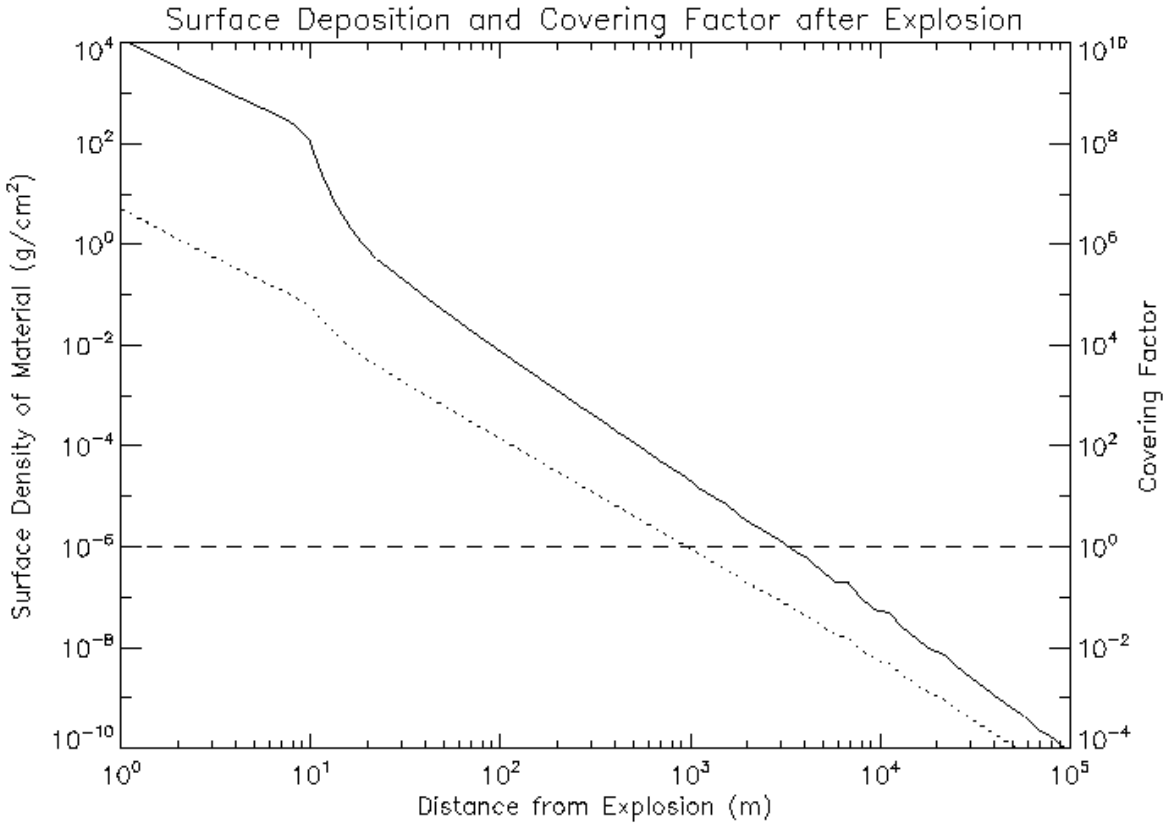

Fig. 4.— Fig. 3. The surface density and covering factor of material deposited by our model minimal TLP versus the distance from the explosion center. The surface density (mass per unit area) is the solid curve and covering factor (total projected particle area per unit area) is dotted, with unit coverage denoted by the dashed line. Away from the crater, there is a near power-law of exponent -2.7 for the surface density of regolith deposited as a function of radius, whereas for covering factor the power-law index is -2.3. Results interior to $r = 10$ m are complicated by the finite size of the crater and much of the large particle material that merely falls near the hypothesized initial position. The ratio of these two curves gives the mass-weighted average particle size, varying as a power law from 3 μm at 20 m radius to 0.04 μm at 100 km.

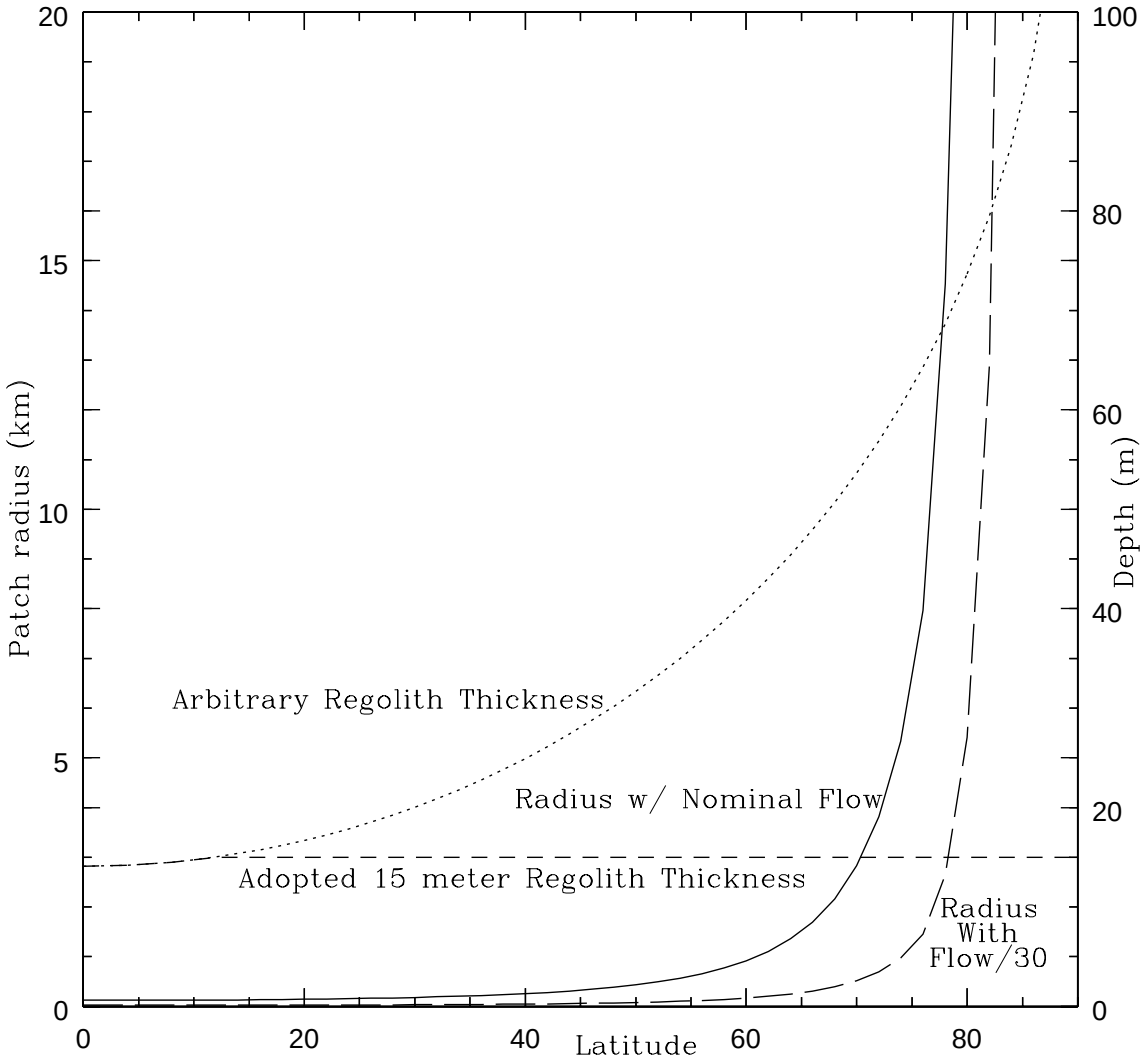

Fig. 5.— The radius of subsurface ice patches and the maximum depth at which we should expect growth of ice, as a function of latitude. The case described in the text corresponds to the solid curve (for ice patch radius - left axis) and the short dashed curve (for ice depth - right axis). The arbitrary 15 m limit is adopted assuming that the low diffusivity regolith overlays a higher diffusivity megaregolith which discourages the growth of ice. If the regolith is actually deeper, or if an ice cap might actually encourage growth of ice at greater depth, in principle the ice layer could extend to the dotted curve (reading the right axis), this would likely encourage the growth of more ice at a given flow rate. (If the regolith were surprisingly deep, the ice patch area might grow larger by a factor roughly the ratio of the dotted curve to the dashed curve.) The long-dashed curve is similar to the solid curve, simply showing the size of the ice patch if the flow rate is reduced by a factor of 30 (to 0.0033 g s^{-1} of water). This curve does not account for time required to reach the equilibrium radius. Smaller than this flow, ice patches might not grow near the equator.

Fig. 6.— Top) Flat-field, dark-corrected but otherwise "raw" image of a typical lunar Near Side image obtained by our robotic imaging monitor. (The image is trimmed to a standard circular region.) Bottom) The difference in signal between the image above and similar one obtained five minutes later. The noise in the residual signal is essentially at the photon shot-noise limit. Because of a slight error in the photometric calibration between the two images there is a very slight ghost of high-contrast global features, especially Imbrium, Humorum and the eastern maria. Note that even bright smaller features e.g., Tycho left and below center, are subtracted nearly identically. Even subtle features not apparent in the image above e.g., an image column acting slightly non-linearly, just left of center, becomes readily apparent. There are also errors along the lunar limb due to the rapid gradient in signal level.

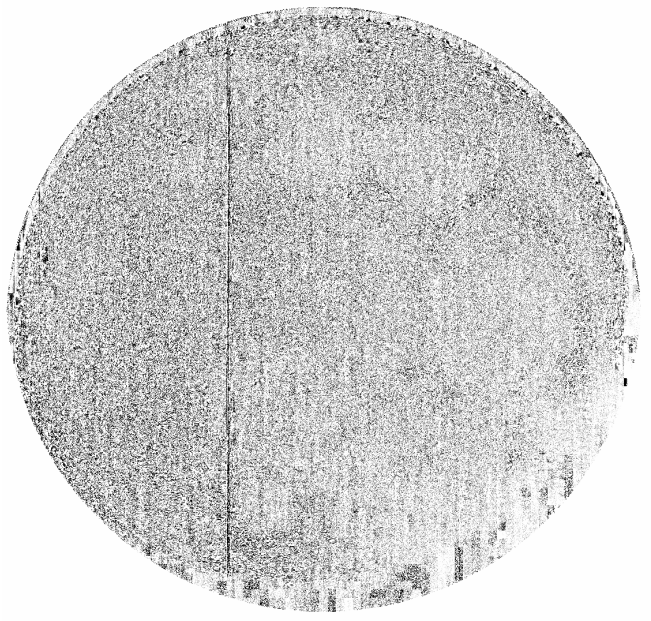

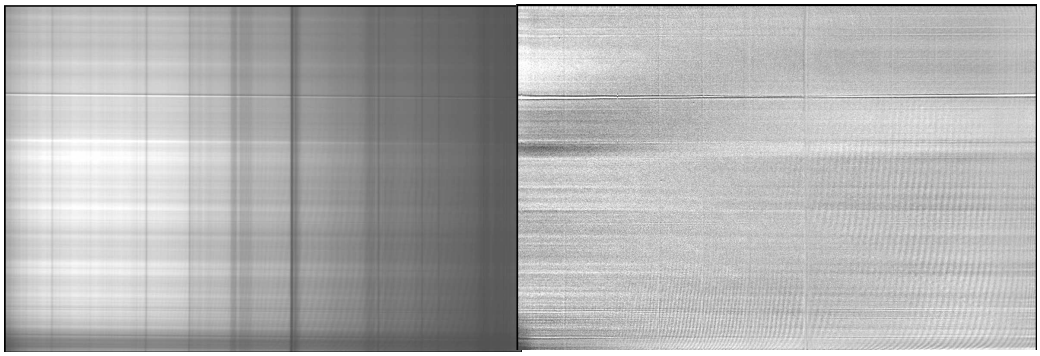

Fig. 7.— **a)** Left: spectrum of an 8-arcmin slit intersecting Aristarchus (bright streak just above center) and extending over Oceanus Procellarum, and covering wavelengths 5500-10500Å, taken by the MDM 2.4-meter telescope; **b)** Right: the residual spectrum once a model consisting of the outer product the one-dimensional average spectrum from Figure 7a times the one-dimensional albedo profile from Figure 7a. The different spectral reflectance of material around Aristarchus is apparent (at a level of about 7% of the initial signal), with r.m.s. deviations of about 0.5%, dominated by interference fringing in the reddest portion, which can be reduced.

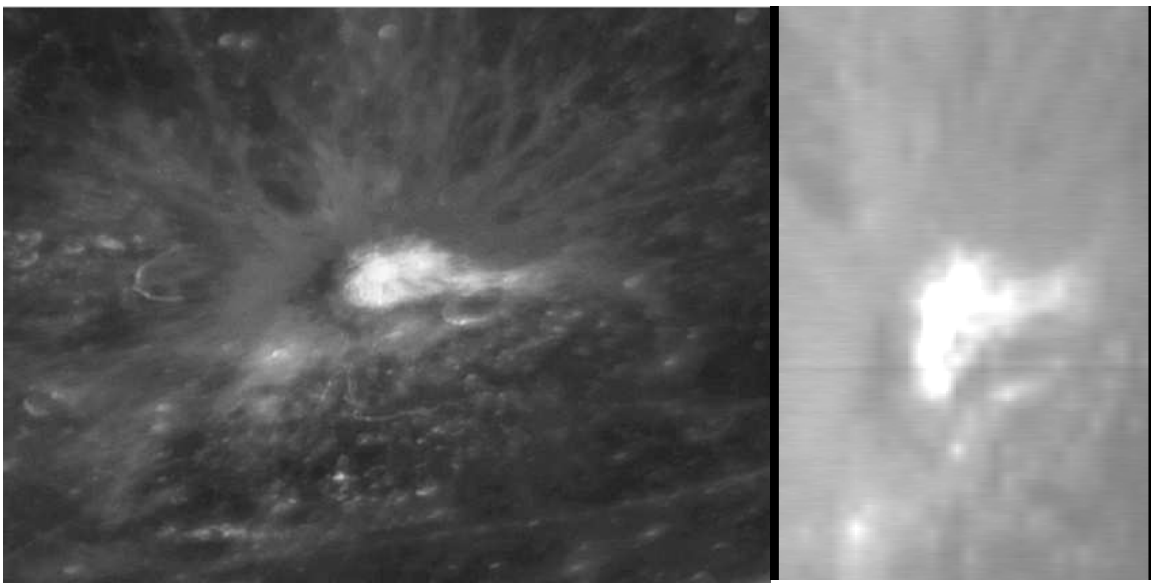

Fig. 8.— **a)** Left: a B-band image of the region around Aristarchus; **b)** Right: an image of Aristarchus in a 3Å-wide centered near 6000Å, constructed by taking a vertical slice through Figure 7a and other exposures from the same sequence of spectra scanning the surface. Any such band between 5500Å and 10500Å can be constructed in the same manner, with resolution of about 1km and 3Å.

Table 1. Summary of Basic Experimental/Observational Techniques Detailed Here

Goal	Detection Method	Channel	Advantages	Difficulties
Map of TLP activity	Imaging monitor, entire nearside, ∼2 km resolution.	optical	comprehensive schedulability; more sensitive than human eye	limited resolution
Polarimetric study of dust	Compare reflectivity in two monitors with perpendicular polarizers	optical	easy to schedule; further constrains dust behavior	requires use of two monitors
Changes in small, active areas	Adaptive optic imaging, ∼100 m resolution	0.95μm, etc.	"on demand" given good conditions	undemonstrated, depends on seeing; covers ∼50 km diameter maximum
	"Lucky Imaging," ∼200m resolution	0.95μm, etc.	on demand given good conditions	low duty cycle, depends on seeing
	Hubble Space Telescope, ∼100 m resolution	0.95μm, etc.	on demand given advanced notice	limited availability; low efficiency
	Clementine/LRO/Chandrayaan-1 imaging, ∼100 m resolution	0.95μm, etc.	existing or planned survey	limited epochs; low flexibility
	LRO/Kaguya/Changé-1 imaging, higher resolution	0.95μm, etc.	existing or planned survey	limited epochs; low flexibility
TLP spectrum	Scanning spectrometer map, plus spectra taken during TLP event	NIR, optical	may be best method to find composition & TLP mechanism	requires alert from TLP image monitor; limited to long events
Regolith hydration measurement	NIR hydration bands seen before vs. after TLP in NIR imaging	2.9, 3.4μm	directly probe regolith/water chemistry; may detect water	requires alert from monitor and flexible scheduling
	Scanning spectrometer map, then spectra taken soon after TLP	2.9, 3.4μm	directly probe regolith/water chemistry; may detect water	requires alert from monitor and flexible scheduling
Relationship between TLPs & outgassing	Simultaneous monitoring: ^{222}Rn α particles by *Kaguya* & optical TLPs	^{222}Rn α & optical	refute/confirm TLP/outgassing correlation; find outgassing loci	optical monitor only covers nearside; more monitors better

Table 1—Continued

Goal	Detection Method	Channel	Advantages	Difficulties
Subsurface water ice	Penetrating radar from Earth	∼430 MHz	directly find subsurface ice with existing technique	ice signal is easily confused with others
	Penetrating radar from lunar orbit	∼300 MHz	better resolution; deeper than neutron or gamma probes	ice signal is easily confused; more expensive
	Surface radar from lunar orbit	>1 GHz	better resolution; study TLP site surface changes	redundant with high resolution imaging?
High resolution TLP activity map	Imagers at/near L1, L2 points covering entire Moon, at 100 m resolution	optical	map TLPs with greater resolution & sensitivity, entire Moon	expensive, but could piggyback on communications network
Comprehensive ^{222}Rn α particle map	Two ^{222}Rn α detectors in polar orbits 90° apart in longitude	^{222}Rn α	map outgassing events at full sensitivity	expensive; even better response with 4 detectors
Comprehensive map of outgas components	Two mass spectrometers in adjacent polar orbits	ions & neutrals	map outgassing events & find composition	expensive; even better with more detectors

Note. — In situ, surface experiments: we refer the reader to work in preparation by AEOLUS collaboration. All methods are Earth-based remote sensing unless specified otherwise. Abbreviations used: TLP = transient lunar phenomena, NIR = near infrared